STRUCTURAL AND KINETIC STUDIES OF CARBONIC ANHYDRASE II AND IX MIMIC INHIBITION

By

JEANNE GABRIELLE QUIRIT

A THESIS PRESENTED TO THE GRADUATE SCHOOL
OF THE UNIVERSITY OF FLORIDA IN PARTIAL FULFILLMENT
OF THE REQUIREMENTS FOR THE DEGREE OF
MASTER OF SCIENCE

UNIVERSITY OF FLORIDA

2009

To my parents who let me bloom

ACKNOWLEDGMENTS

I would first and foremost like to thank my PI, Dr. Robert McKenna, for allowing me to work in his laboratory, for his expertise, encouragement, kindness, and most of all, his patience. His interminable enthusiasm and unwavering guidance has made this seemingly impossible trek towards success all the more possible. I look at Dr. McKenna as more than my superior, but as a true mentor and friend. My thanks and appreciation goes to my committee members, Dr. David Silverman and Dr. Joanna Long, for their support and advice throughout my studies.

Additionally, I would like to extend my deepest gratitude to Jim Rocca who stood by me throughout all the NMR studies. His patience and unyielding support helped me to truly delve into NMR. I would also like to thank Dr. Arthur Robbins who was always willing to answer any questions that I had, whether it be about structure refinement or life in general. I would also like to express my sincere thanks to Dr. Chingkuang Tu for his incessant readiness to help. A special thanks goes to Dr. Jodie Johnson for his useful advice and help. In addition, I am very grateful to all the members of the Silverman Lab and Long Lab who all contributed to the completion of this thesis. Moreover, my utmost appreciation and gratitude goes to all the members of the McKenna lab. The laughter and camaraderie that we shared truly carried me throughout all the difficulties that I encountered.

I gratefully acknowledge the National Science Foundation for financial support through the User Program of the National High Magnetic Field Laboratory (NHMFL), which supported our NMR studies at the Advanced Magnetic Resonance Imaging and Spectroscopy (AMRIS) facility in the McKnight Brain Institute of the University of Florida.

I am immensely grateful to my dear friends, Claudia Sotillo and Katherine Sippel, for their love, their continuous support, and for the indelible memories that we shared. I would also like to thank my family for their encouragement. I will be eternally grateful to my Lola Nene who

never stopped believing in me. Above all, I would like to thank my parents, Marlene and Larry Quirit, who gave me a warm and loving home. They never restricted my abilities to grow and I can honestly say that I would not be who I am today had it not been for my parents. They taught me that nothing is impossible. They are my beacons of strength.

TABLE OF CONTENTS

LIST OF TABLES

LIST OF FIGURES

LIST OF ABBREVIATIONS

CA	Carbonic Anhydrase
HIF-1	Hypoxia-inducible factor-1
AZM	Acetazolamide
BZM	Benzolamide
CHL	Chlorzolamide
EZM	Ethoxzolamide
MZM	Methazolamide
DCP	Dichlorophenamide
SNS	Sympathetic nervous system
TPR	Total Peripheral Vascular Resistance
IOP	Intraocular Pressure
Kapp	Apparent Affinity Constant
HPLC/MS	High Performance Liquid Chromatography/ Mass Spectrometry

Abstract of Thesis Presented to the Graduate School
of the University of Florida in Partial Fulfillment of the
Requirements for the Degree of Master of Science

STRUCTURAL AND KINETIC STUDIES OF CA II AND IX MIMIC INHIBITION

By

Jeanne Gabrielle Quirit

May 2009

Chair: Robert McKenna
Major: Biochemistry and Molecular Biology

α-Carbonic anhydrases (CAs) are zinc-containing metalloenzymes that are primarily responsible for catalyzing the reversible hydration of carbon dioxide to bicarbonate. There are two primary classes of CA inhibitors which are known: the metal-complexing anions and the unsubstituted sulfonamides which attach to the Zn(II) ion of the enzyme via substitution of the non-protein zinc ligand or by the addition to the metal coordination sphere. Currently, therapeutic CA inhibitors have been designed on the basis of sulfonamide, sulfamate, and hydroxamate functional groups that coordinate the active site zinc ion.

Althiazide is a benzothiadiazine derivative that belongs to a class of diuretics used for treating hypertension. Crystallographic studies indicate that the inhibitor binds within the CA II and CA IX mimic active site. However, a lack of electron density surrounding the tail of althiazide suggested that the compound may be degrading within the enzyme and may thus be unstable. NMR studies showed that althiazide is stable under variable pH conditions yet exhibits considerable volatility after its exposure to CA.

HPLC/MS studies were performed to verify the althiazide degradation product that was initially observed in the CA II and CA IX mimic crystal structure and to validate the results from the NMR studies. The results had indicated that a degradation product with a molecular weight

of 285 was in fact present. While the primary causes underlying the deterioration of althiazide cannot be resolved, it is evident that the degradation product acts as a more effective inhibitor than althiazide itself.

Because our knowledge of the binding mechanisms for metal-complexing anions is based on lower resolution data and lower data set completeness, X-ray crystallography was employed to reassess these anion binding patterns. The previously solved crystal structure of bisulfite in adducts with CA II showed that the anion had a puckered conformation (Hakansson, 1992). However, data from the newly solved CAII-bisulfite structure indicates that it has a planar geometry.

Oxygen-18 exchange kinetics via mass spectrometry was used to determine the inhibition constants of various sulfonamide inhibitors. Of the inhibitors tested, benzthiazide had the strongest affinity to CA II whereas hydroflumethiazide showed the weakest inhibitory effects for CA II. Kinetic studies also confirmed that the degraded althiazide product acted as a more potent inhibitor than the non-degraded althiazide compound.

CHAPTER 1
INTRODUCTION

Carbonic Anhydrase Isozymes

α-Carbonic anhydrases (CAs) are widely dispersed, zinc-containing metalloenzymes that catalyze the reversible hydration of carbon dioxide to bicarbonate. CAs are essential in facilitating the transport of protons and carbon dioxide in the intracellular space, in the layers of the extracellular space, and across biological membranes. Moreover, they are associated with an array of physiological functions which include pH regulation, bone resorption, production of biological fluids, ureagenesis, gluconeogenesis, and lipogenesis. In addition, α-CAs are involved in other reactions which include the hydration of cyanate to carbamic acid, the aldehyde hydration to gemdiols, and the hydrolysis of carboxylic or sulfonic acid esters (Briganti et al., 1999, Guerri et al., 2000, Supuran et al., 2004). Presently, there are 15 CA isozymes that have been identified and chiefly differ in their subcellular localization and catalytic activity. CA I-III, VII, and XIII are cytosolic, CA VA and VB are mitochondrial, CA VI is secreted and CA IV, IX, XII, and XIV are membrane-bound.

Structure of Carbonic Anhydrase II

The α-class of CAs is comprised of monomers and has a molecular weight of 30000 Da. CA II is a globular protein that measures approximately 5 x 4 x 4 nm (Lindskog, 1997). The central structural motif of hCA II is characterized by a 10-stranded (βA-βJ) twisted β-sheet, which is flanked by seven α-helices (αA-αG) (Figure 1-1).

The active site is described by a cleft that is about 15 Å deep with a zinc ion located in the internal region. The zinc ion is tetrahedrally coordinated by three histidine residues (His 94, 96, and 119, hCA II numbering) and a bound solvent molecule which acts as the fourth ligand (Figure 1-2). Hydrogen bonds secure the amino acid residues to other groups in the active site

which forms a network of indirect ligands (Lesburg et al., 1995). The metal ion coordinating residues and the indirectly involved coordinating residues remain conserved in all sequenced α-CAs with the exception of residue 244 which stabilizes His-96 through its main chain carbonyl group (Lindskog, 1997). Ten amino acid residues within the α-CAs and the α-CA-related proteins are completely invariable. These consist of Gln 28, Ser 29, Pro 30, Asn 61, Ser 105, Glu 117, Gly 196, Thr 199, Trp 209, and Arg 246. Notably, Glu 117 and Thr

199 act as indirect ligands in the active enzymes (Figure 1-3). Thr199 hydrogen bonds with the zinc-bound hydroxide and allows it to orient it for optimal nucleophilic attack on the incoming CO_2.

Carbonic Anhydrase Catalytic Mechanism

CA catalyzes the interchange of CO_2 to HCO_3^- in a two-step mechanism. In the first step, a CO_2 substrate is trapped in a hydrophobic pocket (Equation (1-1) (Lindskog, 1997).

$$CO_2 + EZnOH^- \Leftrightarrow EZnHCO_3^- \overset{H_2O}{\Leftrightarrow} EZnH_2O + HCO_3^- \quad (1\text{-}1)$$

The catalytic substrate CO_2 binds to a hydrophobic pocket that is about 3-4 Å from the zinc ion (Messerschmidt, 2001). Studies have shown that the pocket is composed of residues Val1 21, Val 143, Leu 198, Val 207, and Trp 209. In the active site, the CO_2 interacts with the amide nitrogen of Thr 199 in a hydrogen-bonding association and thus displaces a water molecule (Messerschmidt, 2001). This action occurs prior to a nucleophilic attack on the substrate carbon by the zinc-bound water molecule to generate bicarbonate (Figure 1-4). Subsequently, a different active-site water molecule removes the bicarbonate from the zinc ion, thus completing the first-half reaction (Equation 1-1).

The second step in carbonic anhydrase catalysis is the rate-limiting step. A proton is transferred from the zinc-bound water molecule to the proton shuttling residue His64 via a series

of well-ordered hydrogen-bonded water molecules (Equation 1-2) (B is defined as the bulk solvent) (Lindskog, 1997).

$$EZnH_2O + B \Leftrightarrow EZnOH^- + BH^+ \quad (1\text{-}2)$$

Based on the three-dimensional structure of hCA II, the proton shuttling residue, His 64 resides in the active-site region with its imidazole ring in the 'in' conformation which is positioned 7 Å away from the zinc ion (Eriksson et al., 1988). The intramolecular proton transfer proceeds in a stepwise fashion. Initially, a proton is transferred from the zinc-bound water molecule to a nearby hydrogen-bonded water molecule. Subsequently, a different proton is transferred from this water molecule to another hydrogen-bonded water molecule which then transfers a different proton to the His 64 (Figure 1-5). After the second half of the reaction, another cycle of catalysis can continue because a zinc-bound hydroxyl group is regenerated (Messerschmidt, 2001). The side chains of residues Tyr 7, Asn 62, Asn 67, and Thr 200 also participate in stabilizing several active site waters that are thought to comprise the solvation structure contributing to the efficient proton transfer to His 64 (Figure 1-5) (Messerschmidt, 2001). It has been demonstrated that site-directed mutagenesis of these residues has considerable effects on proton transfer rates. The active site can exist as a high pH form that is dynamic in the hydration of carbon dioxide and a low pH form that is active in the dehydration of bicarbonate (Supuran et al., 2004).

Carbonic Anhydrase II Physiological Function

CA II has a maximum CO_2 hydration turnover rate of about 10^6 sec^{-1} at pH 9 and 25˚C and is prevalent in various tissue types with large concentrations located in red blood cells where it is involved in respiration (Lindskog, 1997). A CA II deficiency has been implicated in osteopetrosis, renal tubular acidosis and cerebral calcification which demonstrates the

significance of this isozyme in the bone, kidney, and brain (Sly et al., 1983). CA II is involved in bone resorption as well as HCO_3^- reabsorption and acidification via the proximal renal tubules in the kidney; In addition, it provides H^+ in the distal regions of the nephron which regulate distal urinary acidification. Studies have further demonstrated the importance of CA II in the mental retardation and brain calcification which was observed in over 90% of affected patients (Sly et al., 1983).

Carbonic Anhydrase IX Background

Among the various CA isoforms, CA IX is highly overexpressed in tumor cells which may be attributed to its transcriptional activation by hypoxia via the transcription factor hypoxia-inducible factor-1 (HIF-1) (Thiry et al., 2006). CA IX is implicated in processes connected with cancer progression and response to therapy. Consequently, these properties make CA IX an instrumental marker for hypoxia and a predictor for many cancers. It has been reported that CA inhibitors serve as anti-glaucoma drugs. Furthermore, CA inhibitors may potentially serve as anti-cancer, anti-infective drugs, and as a novel therapy for Alzheimer's disease (Thiry et al., 2006).

It has been proposed that CA IX aids in cell proliferation, cell adhesion, and malignant cell invasion. It has limited expression in normal tissue, predominantly expressed in the gastrointestinal tract. CA IX is confined to the basolateral surfaces of all types of epithelial cells. It thus participates in keeping the gastric mucosa intact and maintaining a balance between cell differentiation and proliferation. It has high levels of expression in a number of cancers that stem from CA IX-negative tissues which include renal, lung, cervical, ovarian, esophageal, and breast carcinomas.

Mature CA IX can be characterized by its four domains which are comprised of an N-terminal proteoglycan-like domain (PG), a CA catalytic domain (CA), a transmembrane helical

segment, and a short intracytoplasmic tail (Figure 1-7) (Thiry et al., 2006). HIF-1 is a heterodimer that is comprised of an inducible subunit (HIF-1α) and a constitutively expressed subunit (HIF-1β) (Figure 1-6). Under hypoxic conditions, HIF-1α becomes expressed and activates the HIF-1 complex. During normal conditions, proteins that have an oxygen-dependent prolyl-4-hydroxylase domain (PHD) hydroxylate proline residues in the oxygen-dependent degradation domain of HIF-1α. The hydroxylated HIF-1α to hydrogen bond with side chains on the von Hippel-Lindau tumor suppressor protein (pVHL) consequently becoming polyubiquitinated and eventually targeted for degradation by the 26S proteasome (Thiry et al., 2006). Hypoxic conditions hamper the binding of pVHL to HIF-1α which causes HIF-1α to build up and dimerize with the constitutive HIF-1β subunit. In this manner, hypoxia constricts proline hydroxylation and inactivates the PHDs. HIF-1 activation is a result of the interaction made between HIF-1α and HIF-1β. Targets that contain hypoxia-responsive element (HRE) sites subsequently become expressed. CA IX becomes upregulated due to the constitutive HIF activation. Pastorek et al. was the first to clone and examine a cDNA coding for the human CA IX protein (Pastorek et al., 1994). This group subsequently characterized the CA9 gene in 1996 (Hilvo et al., 2008). This study showed that CA IX shared similar traits with the keratan sulfate attachment domain of a large human aggregating proteoglycan (Hilvo et al., 2008).

CA IX Biological Characterization

Since CA IX is a membrane protein, there are difficulties in crystallizing and structurally analyzing it and thus its biochemical characterization remains incomplete. However, various genetic techniques have been developed to determine the catalytic properties, oligomerization, and post-translational modifications of CA IX. Hilvo et al., produced two recombinant forms of soluble CA IX forms using the baculovirus-insect cell expression system. Both forms lacked the

small transmembrane and intracytoplasmic domains and both proteins had a CA IX signal sequence (Hilvo et al., 2008). Studies on the oligomerization and stability of the proteins indicated that both recombinant forms produce dimers that are stabilized by intramolecular disulfide bonds. Mass spectrometry experiments demonstrated that CA IX forms an intramolecular S-S bridge connecting Cys119 to Cys299 and an N-linked glycosylation site on Asn309 that has high mannose-type glycan structures (Hilvo et al., 2008). Additional studies showed that another O-linked glycosylation site exists on Thr78.

Roles of CA IX in Cancer Biology

CA IX is perinecrotic which is characteristic of hypoxia-regulated proteins. Typically, necrosis occurs in areas that are far from the functional blood vessel. Cells are unable to survive because they endure severe hypoxia. Conversely, cells that are closer to the functional blood vessel (in the perinecrotic regions) and do not suffer from such astringent conditions can lead to the induction of HIF-1 targets such as CA IX and thus are able to adapt to low-oxygen conditions (Thiry et al., 2006).

The overexpression of CA IX in tumors creates a change in the tissue pH. While normal tissues have an extra-cellular matrix pH of about 7.4, the majority of hypoxic tumors are acidic with a pH of about 6. A study led by Pastorekova demonstrated the role of CA IX in the acidification processes of hypoxic tumors (Svastova, 2004). They used Madin-Darby canine kidney epithelial cells that constitutively expressed human CA IX and proved that the protein actually reduces the extracellular pH of cultivated cells (Svastova, 2004). Furthermore, obliterating the active site in the catalytic region of CA IX had consequently reduced the acidification of the environment (Svastova, 2004).

Tumor cells reduce their extracellular pH by generating lactic acid and by hydrating CO2 which is catalyzed by CA IX. A low extracellular pH has been correlated with tumorigenic

transformation, chromosomal rearrangements, extracellular matrix breakdown, migration and invasion, induction of cell growth factors, and protease activation (Supuran et al., 2004, Stubbs et al., 2000).

CA IX Drug Therapy Implications

The acidification of the extracellular region of tumor cells has important consequences in chemotherapy (Vukovic & Tannock, 1997). An acidic environment may reduce the uptake of an alkaline anticancer drug which ultimately results in chemoresistance (Raghunand *et al.*, 1999). The majority of anticancer drugs travel via active transport or passive diffusion into cells where they are often metabolized. Since all of these processes are sensitive to variable pHs, the cytotoxic activity of anticancer drugs may be dependent on both the intracellular and extracellular pH (Stubbs *et al.*, 2000).

Weakly ionized drugs enter cells in their non-ionized form via passive diffusion. These drugs generally localize across the cell membrane into a region where it shares the same ionization state. Several strategies have been developed to change the intracellular and extracellular pH in tumor cells. The cytotoxic effectiveness of weakly basic drugs like mitoxantrone, paclitaxel and topotecan have shown improvement after enhancing the extracellular pH(Vukovic & Tannock, 1997). Inhibitors that are targeted for CA IX may also enhance the efficacy of weakly basic drugs.

Recently, an interest in CAs and their sulfonamide inhibitors as cancer treatments has arisen (Supuran *et al.*, 2004, Pastorekova, 2004b, Pastorekova *et al.*, 2004a, Svastova *et al.*, 2004). It has been proven that many powerful inhibitors derived from acetazolamide, ethoxzolamide and benzenesulfonamides impede the proliferation of several tumor cell lines both *in vitro* and *in vivo* (Vullo *et al.*, 2005, Supuran *et al.*, 2001). Since many of the cell lines

tested expressed either CA IX, CA XII, or both, this suggests that the anti-proliferative effects of sulfonamides are regulated by the inhibition of these isoforms (Supuran *et al.*, 2001).

Acetazolamide can reduce tumor metastasis *in vivo* by inhibiting the expression of aquaporin, a water channel protein that may be involved in vascular permeability and interstitial fluid pressure in tumors, and inhibiting CA IX, XII, and II (Supuran *et al.*, 2004). Aquaporin may also mediate the transport of CO_2. Therefore, preventing its function via a sulfonamide might account for the cytotoxic effects of these drugs. The anti-tumor effects of CA inhibitors can also be attributed to their inhibition of other CA isozymes such as CA II or CA V, which are indirectly involved in carboxylation reactions such as lipogenesis, nucleotide biosynthesis, and gluconeogenesis (Supuran *et al.*, 2004).

CA IX Mimic

The difficulties in crystallizing CA IX have prompted the need to develop a means of studying its active site for rational drug design. A duplicate of the CA IX active site has been produced by mutating two residues in CA II (A65S-N67Q CA II) so that it emulates the active-site of CA IX (Figure 1-8) (Genis et al., 2009). The CA IX mimic was expressed and kinetically and crystallographically characterized by itself and in adducts with various established inhibitors which included acetazolamide (AZM), benzolamide (BZM), chlorzolamide (CHL), ethoxzolamide (EZM), and methazolamide (MZM). These studies indicated that the CA IX mimic inhibition profiles paralleled the wild-type CA IX (Genis et al., 2009).

Clinical Applications of Carbonic Anhydrase Inhibitors

Glaucoma is a degenerate eye disease marked by elevated intraocular pressure (IOP), which leads to irreversible damage to the optic nerve head and consequently a gradual loss of visual function. AZM, MZM, EZM, and dichlorophenamide (DCP) are clinically established inhibitors used for treating glaucoma (Sly & Hu, 1995). These drugs function by inhibiting CA

II and IV which are found in the ciliary processes of the eye. Inhibition of these isozymes results in the reduction of bicarbonate and aqueous humor secretion and of increased IOP. However, because CA II and IV are prevalent in other tissues and organs, consumption of these drugs produces undesired side effects like numbness and tingling of extremities, metallic taste, depression, fatigue, malaise, weight loss, decreased libido, gastrointestinal irritation, metabolic acidosis, renal calculi and transient myopia (Supuran et al., 2004). Topically effective CAIs have been produced to circumvent these side effects.

Histochemical studies in the parietal cells and surface epithelial cells indicated that gastric mucosa contained CA (Davenport, 1938). Additional immunhistochemical techniques have shown that CA II is the primary isoform present in the astric mucosa. Gastric acid is neutralized by gastroduodenal bicarbonate which is secreted by the surface epithelial cells (Parkkila & Parkkila, 1996a, b).

Classes of Carbonic Anhydrase Inhibitors

There are two primary classes of carbonic anhydrase inhibitors which are known: the metal-complexing anions and the unsubstituted sulfonamides which attach to the Zn(II) ion of the enzyme via substitution of the nonprotein zinc ligand or by the addition to the metal coordination sphere, thus creating a trigonal-bypyramidal construct (Lindskog, 2000)(Pertini et al. 1982; Lindskog and Silverman 2000).

Carbonic Anhydrase Inhibition Kinetics

In regards to kinetics and coordination behavior, the inhibition mechanism is a multifaceted topic (Bertini et al., 1983). Since CA exists in the acidic and basic form, the binding of the inhibitor to the enzyme is pH dependent. The pKa describes the equilibrium for each isozyme: 7.0 for CA I (Pocker & Tanaka, 1978, Pocker & Sarkanen, 1978), 7.0 for CA II (Baird et al., 1997), 8.0 for CA III (Rowlett et al., 1991), 7.1 for CA IV (Baird et al., 1997), 7.4

for CA V (Heck et al., 1994), 6.3 for CA IX (Wingo et al., 2001). The relationship between the inhibitor and the enzyme is described by Equation 1-3:

$$E + I \Leftrightarrow EI \quad (1\text{-}3)$$

Hence, the binding of the inhibitor to the enzyme is characterized by the inhibition constant (Equation 1-4).

$$KI = [EI]/[E][I]. \quad (1\text{-}4)$$

The apparent affinity constant of the inhibitor (Kapp) takes into consideration the pH fluctuations during the enzyme-inhibitor interaction and thus corrects the KI. It is described by Equation 1-5 (Bertini et al., 1982, Pocker & Sarkanen, 1978):

$$K_{app} = KI/(1+(Ka_{Enz}/[H+])) \quad (1\text{-}5)$$

Table 1-1 shows that OH- has the strongest affinity for the Zn(II) ion of hCA II. This is followed by CN-, HS-, SCN-, CNO-, and N3- (Pertini, 1981) .

After considering the pH dependence for the binding of inhibitors to native and Co(II)-substituted CA, Bertini and Luchinat proposed three different classes of CA inhibitors—A, B, and C (Bertini, 1983).

Class A, B, and C Inhibitors

The Kapp of Class A Inhibitors is represented in Figure 1-10 and is comprised of mononegative anions that are conjugated bases of strong acids (X-, NO3-, ClO4-, CNO-/NCO-, SCN-, etc (Bertini, 1983, Coleman, 1975). They bind the acidic form of the enzyme with a progressive decrease in binding affinity at alkaline pHs. This is a consequence of the inhibitor competing with the hydroxide ion. This binding mode is also observed in aniline (Bertini, Luchinat et al., 1977), N-methylimidazole (Alberti et al., 1981), and by the bicarbonate ion (Bertini, 1983).

Class B Inhibitors exhibit a bell-shaped curve for log Kapp vs. pH (Figure 1-10) (Bertini, 1983). When the inhibitor is in its anionic form, it binds the acidic form of the enzyme. Conversely, when the inhibitor is in its neutral form, it binds to the alkaline form of the enzyme. This class consists of CN- (Thorslund & Lindskog, 1967), HS (Pocker & Stone, 1968, Thorslund & Lindskog, 1967), the sulfonamides (Kernohan, 1966, Thorslund & Lindskog, 1967, Taylor et al., 1970) and the hydrated trichloroacetaldehyde (Bertini et al., 1979a) and α-amino acids in their zwitterionic form (Bertini, Canti et al., 1977).

The pH dependence of Kapp for Class C Inhibitors fall between Class A and Class B (Figure 1-10) (Bertini, 1983). Inhibitors in this category bind to the enzyme over a broad range of pH values which is a result of their unique structural and ionizing properties. This class is comprised of imidazole, 1,2,4-triazole, and 1,2,3-triazole (Alberti et al., 1981).

Anions

A wide variety of monovalent anions inhibit CA. Previous studies on the pH dependence of inhibition have indicated that anionic inhibitors bind to the metal ion and impede the formation of the hydroxyl moiety, which is essential for the catalysis of CO_2 hydration (Lindskog, 1997). Anions form a tetrahedral geometry or pentacoordinated network by displacing the zinc-bound solvent molecule (Bertini, Canti *et al.*, 1977).

Crystallographic studies have indicated that Glu 106, Thr 199, and the zinc-bound solvent are critical players in the active site (Figure 1-9). Since Glu 106 becomes ionized it acts as a hydrogen bond acceptor with Thr 199 (Lindskog, 1997). The hydroxyl group of Thr 199 binds to the zinc-bound solvent by accepting a hydrogen atom. The zinc-bound H_2O or OH^- hydrogen bonds with a water molecule in a hydrophobic region and to the peptide NH of Thr 199

(Lindskog, 1997). This hydrogen-bonded network influences the manner in which inhibitors bind (Liljas *et al.*, 1994).

Anionic Inhibitor Binding Mechanism

Inhibitors that have a protonated ligand atom replace the metal-bound solvent molecule while still preserving the tetrahedral geometry and the hydrogen bond with the hydroxyl group of Thr 199. The majority of anions lacking a protonated ligand do not abstract the zinc-bound solvent molecule, however, it still many still continue to hydrogen bond with the NH moiety of Thr-199 (Figure 1-9) (Lindskog, 1997). In this case, the metal ion is pentacoordinated and is about 1.9 Å to 3.4 Å away from the inhibitor (Lindskog, 1997). NMR studies of thiocyanate, formate, and acetate complexes of bovine Co^{2+}-CA II validate this pentacoordinated geometry (Lindskog, 1997). The metal poisons such as CN^- and NCO^- can be categorized under this group of inhibitors (Figure 1-9).

Another class of anions adheres to the metal ion and transposes the zinc-bound water molecule, but does not hydrogen bond with Thr-199. The metal ion then becomes tetrahedrally coordinated. The halogenide ions such as Br and I as well as azide can be categorized as these type of inhibitors (Figure 1-9) (Jonsson et al., 1993). These inhibitors disrupt the hydrogen-bonded water network that is coordinated by Glu 106 and Thr 199 (Liang et al., 1993).

Divalent anions like SO_4^{2-} do not exhibit any inhibitory effects on CA. Binding is impeded by the negative charge of Glu 106 and the hydrogen-bond requirements between Glu 106 and Thr 199. Studies of CA II where Glu 106 was mutated to Ala or Gln show that SO_4^{2-} bound tightly to the zinc ion and thus substantiates this view (Lindskog, 1997).

The general agreement on anionic inhibition is that anions act as noncompetitive inhibitors for both the hydrase and the esterase activity of CA, but act as a competitive inhibitor with respect to the anionic product bicarbonate (Lindskog, 1971). The anionic binding affinity for

CA varies between the isozymes. CA I is more strongly inhibited by anions than CA II (Maren et al., 1976) which shares a similar behavior with CA IV (Baird et al., 1997). CAs III, VI, and IX are moderately inhibited by anions (Engberg & Lindskog, 1984, Lindskog et al., 1984, Murakami & Sly, 1987, Rowlett et al., 1991, Wingo et al., 2001).

Sulfonamides

Sulfonamides, class B inhibitors, bind to the Zn(II) ion as anions via a nitrogen atom, generating a tetrahedral geometry (Figure 1-11). Thr 199 and Glu 106 stabilize the sulfonamide moiety through a network of hydrogen bonds. NMR studies of $_{111}Cd^{2+}$ or $_{113}Cd^{2+}$ substituted CA complexed with 15N-labelled inhibitors provide support for N-coordination (Supuran et al., 2004). Crystallographic studies have also indicated that the NH group of the ionized sulfonamide replaces the zinc-bound water molecule and interacts with the hydroxyl moiety of Thr 199 through hydrogen bonds (Lindahl, 1991, Stams et al., 1996, Stams & Christianson, 2000, Masereel et al., 2002, Abbate et al., 2003, Supuran, 2003). One of the oxygen atoms hydrogen bonds to the peptide NH of Thr 199 while another oxygen atom is coordinated to the zinc ion (Bertini et al., 1982, Lindskog, 2000, Supuran, 2003, 2000, 2002). The aromatic group of the inhibitor interacts with various hydrophilic and hydrophobic residues in the active site.

The sulfonamide's ability to bind to CA is related to the acidity of the sulfonamide group. Studies of the binding affinities of aliphatic sulfonamides depict this view. $CH_3SO_2NH_2$, with a pKa of 10.5, has a dissociation constant of 0.3 mM (Maren & Wiley, 1968) while the fluorinated counterpart, CF3SO2NH2, with a pKa of 5.8, has a dissociation constant of 2 nM (Maren et al., 1993). The crystal structure of this inhibitor complexed with human CA II depict the trifluoromethyl group situated within a hydrophobic pocket and interacting with Val 121, Val 143, Leu 198, and Trp 209 (Figure 1-12) (Hakansson & Liljas, 1994).

The crystal structure complex of human CA II and acetazolamide, a clinically established inhibitor of CA, contains a thiadiazole ring which makes van der Waals interactions with Val 121, Leu 198, and Thr 200 while the carbonyl oxygen of the amido group hydrogen bonds with the side-chain amide of Gln 92; the methyl group interacts with Phe 131 (Figure 1-13) (Vidgren et al., 1990).

Comparison of CA Inhibition Via Anions and Sulfonamides

Both anions and sulfonamides bind to CA in the stoichiometric ratio of 1:1 (Bertini et al., 1982, Bertini, 1983). The binding of inhibitors to the enzyme can result in significant changes to the electronic and magnetic properties of both the metal ion and the inhibitor.

1H-NMR studies on Co-CA show that upon the binding of inhibitors to the cobalt protein, the histidines stay coordinated (Bertini, 1983). As a result, inhibitors can yield tetrahedral products, pentacoordinated products, or a balance of the two (Bertini, 1983).

Nuclear magnetic resonance spectroscopy has proven to be an effective tool for elucidating the inhibition mechanism of CA and the coordination behavior of various anionic and neutral inhibitors to the metal ion of the active site. Anions like CN^-, NCO^-, SH^- and inhibitors like aniline, anthranilate, trichloroacetaldehyde, thiadiazole, imidazole (at high pH), 1,2,4-triazole, tetrazole and all the sulfonamides produce pseudotetrahedral species (Bertini, 1983). A pentacoordinated species is observed for anions such as SCN^-, HSO_3^-, NO_3^-, I^-, $Au(CN)_2^-$, $Ag(CN)_2^-$, formate, acetate, bromoacetate, oxalate, malonate, succinate, glutarate, and ligands which include glycine, L(+)-aniline, D(-)-alanine, 2,4-pentanedione, and 1,2,3-triazole. HCO_3^-, F^-, Cl^-, Br^-, N_3^-, phosphate and benzoate anions and imidazole at low pH yield four-to five-coordinated species (Banci, 1989, Bertini, 1981, Bertini, Luchinat et al., 1977).

Thiazides

Thiazides, which are a recently characterized group of CA inhibitors, belong to a class of diuretics and are frequently used for the treatment of hypertension. When administered acutely, they reduce blood pressure by diminishing the plasma volume, depressing the venous return, and reducing the cardiac output and blood pressure (Hughes, 2004, Dustan, Cumming *et al.*, 1959). In addition, the sympathetic nervous system (SNS) regulates an increase in the total peripheral vascular resistance (TPR) and the rennin-angiotensin-aldosterone system becomes activated (Corcoran *et al.*, 1959). Thiazides are also known to block the Na^+/Cl^- reabsorption from the distal convoluted tubules in the kidneys by impeding the thiazide-sensitive Na^+/Cl^- symporter (Dustan, Page *et al.*, 1959, Dollery *et al.*, 1959, Conway & Lauwers, 1960). They are involved in the loss of potassium and a rise in serum uric acid and have inhibitory effects on renal carbonic anhydrase (Hughes, 2004).

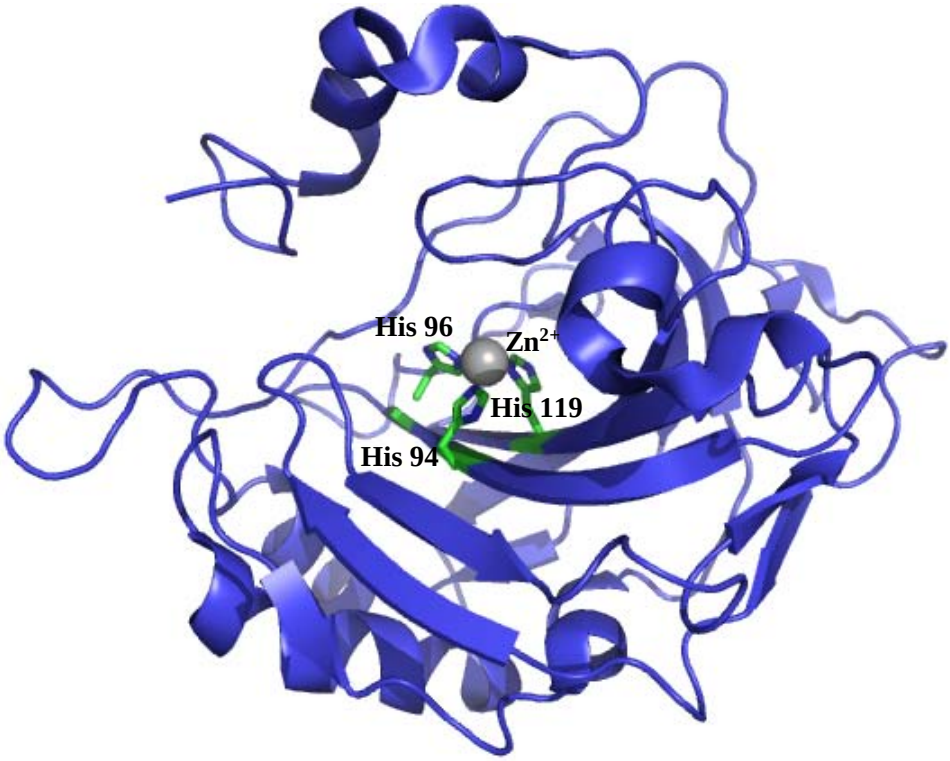

Figure 1-1. Structure of human CA II. Ribbons and arrows convey helices and β-strands, respectively. The Zn(II) ion is labeled and is shown as a gray sphere with the three coordinating histidyl ligands. The figure was generated in PyMol (DeLano, 2002).

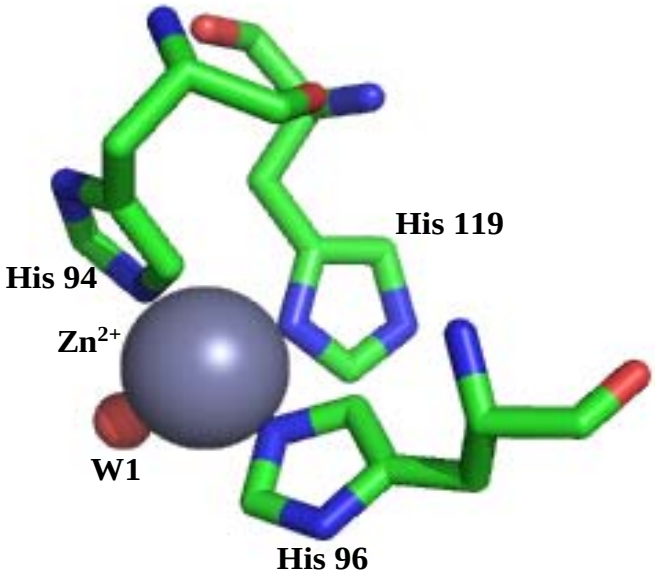

Figure1-2. The tetrahedral coordination of zinc in the active site of wt hCAII. The Zn2+ atom is labeled and shown as a gray sphere; side chain residues are labeled and atom coloring is depicted as follows: carbon (green), oxygen (red), nitrogen (blue). Water molecules are labeled and shown as a red sphere. The figure was generated in PyMol (DeLano, 2002).

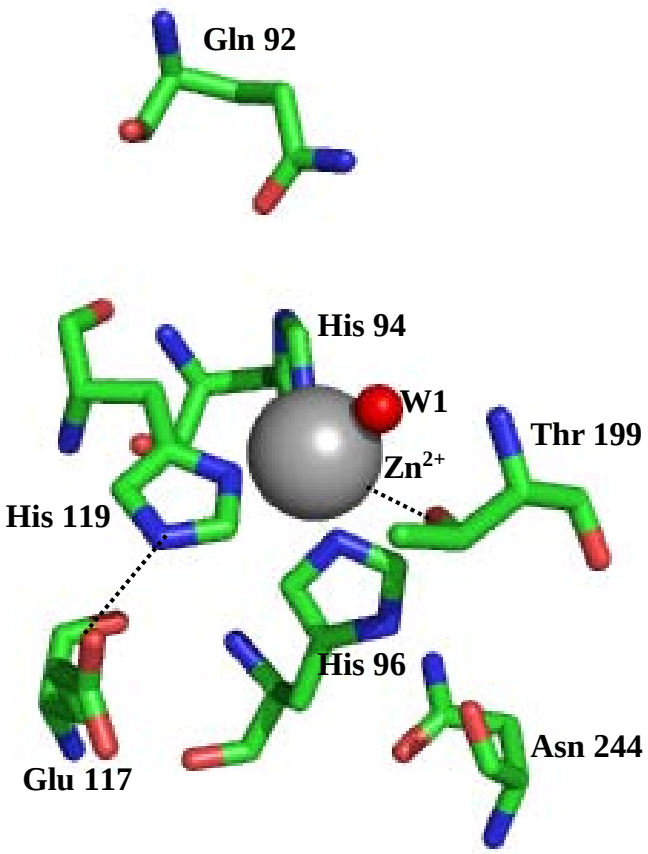

Figure 1-3. View of Zn(II) center in wt hCA II displaying direct and indirect ligands. The Zn2+ atom is labeled and shown as a gray sphere; side chain residues are labeled and atom coloring is depicted as follows: carbon (green), oxygen (red), nitrogen (blue). Water molecules are labeled and shown as a red sphere. The figure was generated in PyMol (DeLano, 2002).

Figure 1-4. Schematic representation of carbonic anhydrase catalytic mechanism of action.

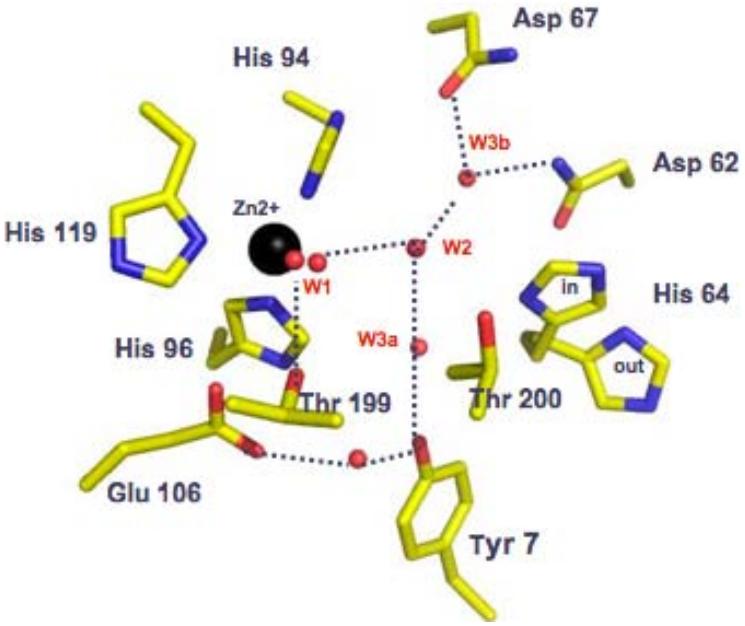

Figure 1-5. Water network depicted in the hCA II active site. The Zn2+ atom is labeled and shown as a black sphere; side chain residues are labeled and atom coloring is depicted as follows: carbon (yellow), oxygen (red), nitrogen (blue). Water molecules are labeled and shown as a red sphere. The figure was generated in PyMol (DeLano, 2002).

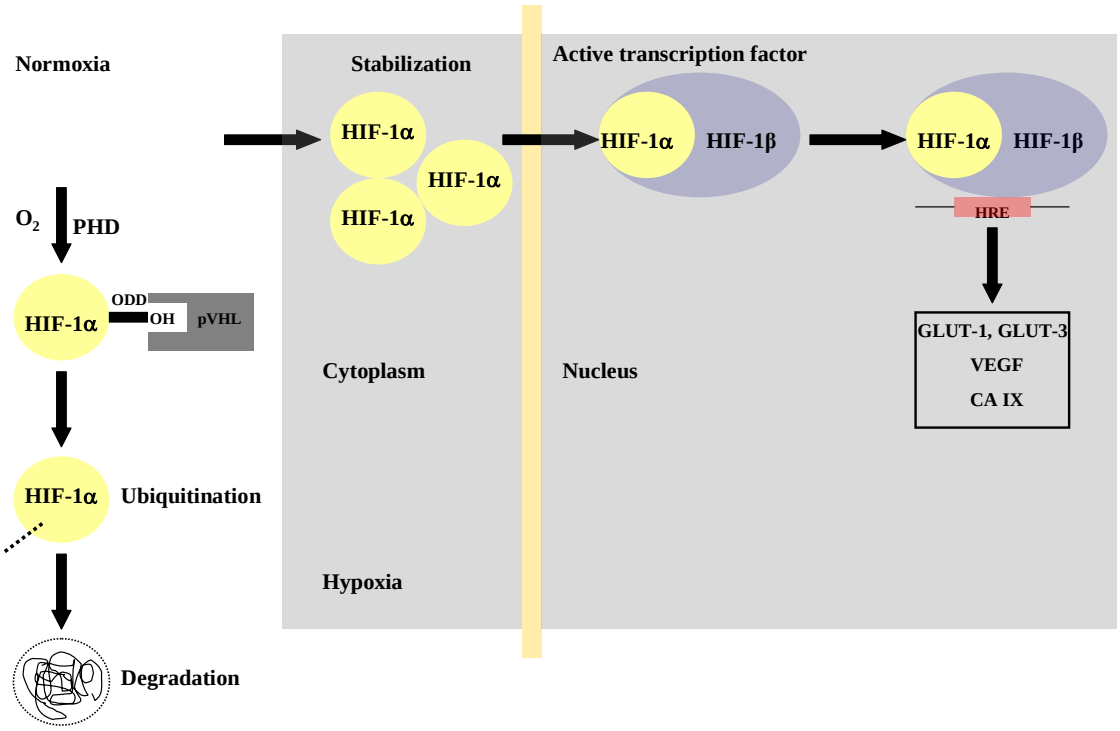

Figure 1-6. Hypoxia-induced gene expression regulation. [Adapted from Thiry et al., 2006. Targeting tumor-associated carbonic anhydrase IX in cancer therapy. Trends Pharmacol. Sci. (Page 567, Figure 1). Drug Design and Discovery Center, University of Namur, Namur, Belgium.]

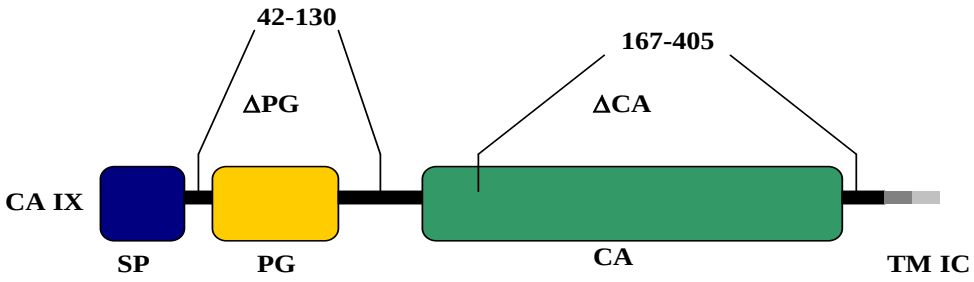

Figure 1-7. CA IX protein domain. [Adapted from Thiry et al., 2006. Targeting tumor-associated carbonic anhydrase IX in cancer therapy. Trends Pharmacol. Sci. (Page 568, Figure 1). Drug Design and Discovery Center, University of Namur, Namur, Belgium.]

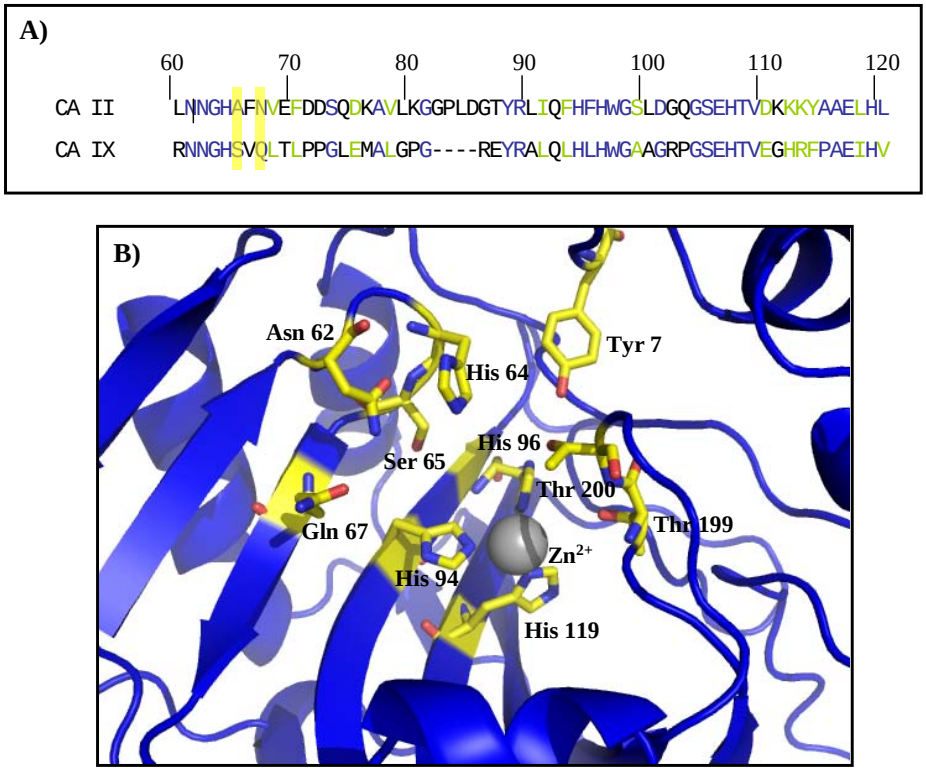

Figure 1-8. A) CA II and CA IX amino acid sequence alignment beginning with residue 60 to 120 (CA II numbering). Conserved residues His64, His94, His96, His119, and all active-site residues are shown in blue. Active-site variants, residues 65 and 67, are highlighted in yellow. Alignment performed using Clustal W (Thompson, 1994).B) Crystal structure of CA IX mimic. Zn 2+ atom is shown as a gray sphere. Side chain residues are labeled and atom coloring is as follows: carbon (yellow), oxygen (red), nitrogen (blue). Figure was generated in PyMol (DeLano, 2002). [Adapted from Genis et al. 2009. Design of a carbonic anhydrase IX active-site mimic to screen inhibitors for possible anticancer properties. Biochemistry (Page1326, Figure 1) University of Florida, Gainesville, Florida.]

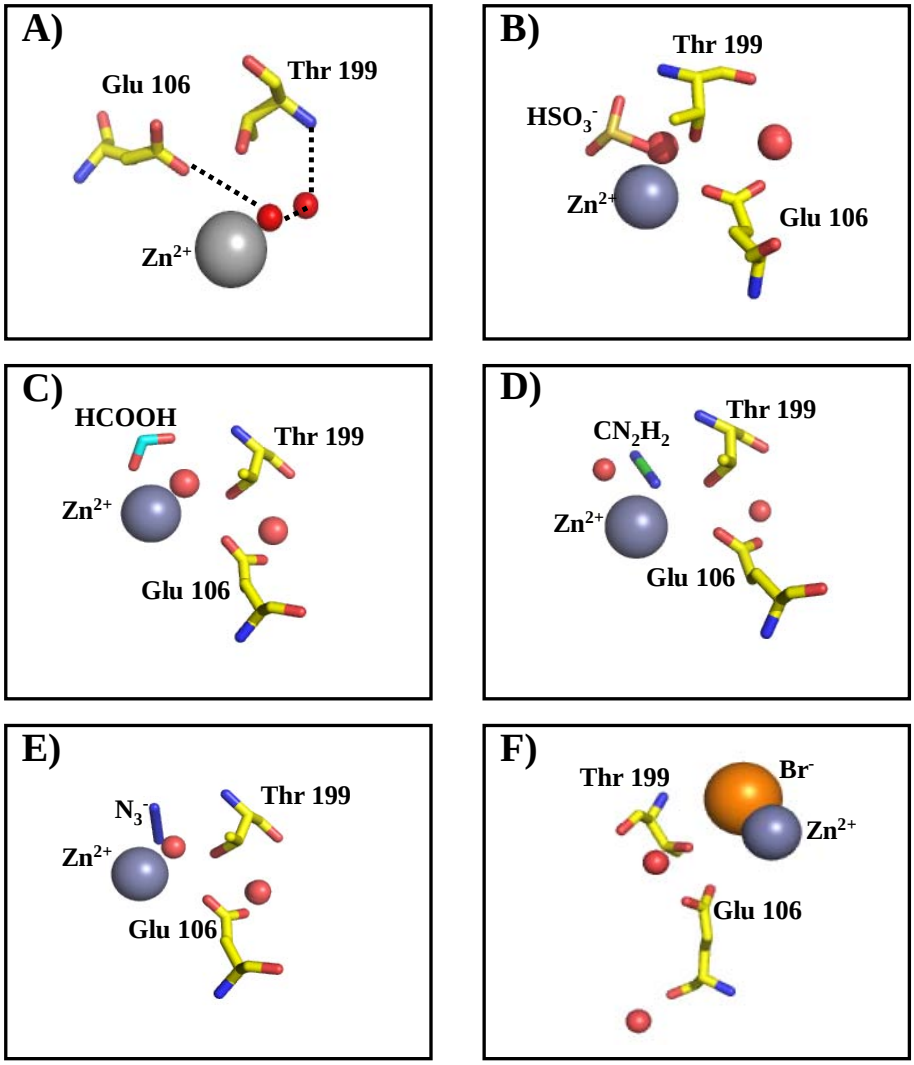

Figure1-9. Crystal structures of metal-complexing anions in CA II active site. A)uninhibited CA II. B) bisulfite C) formic acid D) cyanamide E) azide F) bromide; Zn^{2+} atom is shown as a gray sphere. Water molecules are shown as red spheres. Side chain residues are labeled and atom coloring is as follows: carbon (yellow), oxygen (red), nitrogen (blue). Anions are labeled. Figure was generated in PyMOL(DeLano, 2002).

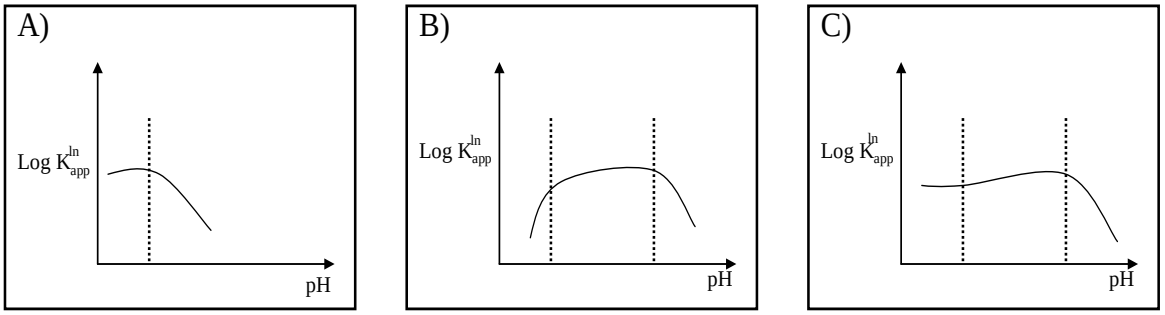

Figure 1-10.Figure depicts the pH dependence of the apparent affinity constants of classes A, B and C carbonic anhydrase inhibitors; the dashed lines represent the enzyme pKa (left) and the inhibitor pKa (right). [Adapted from Bertini, I., and Luchinat, C. 1983. *Accounts of Chemical Research* **16**, 272-290.]

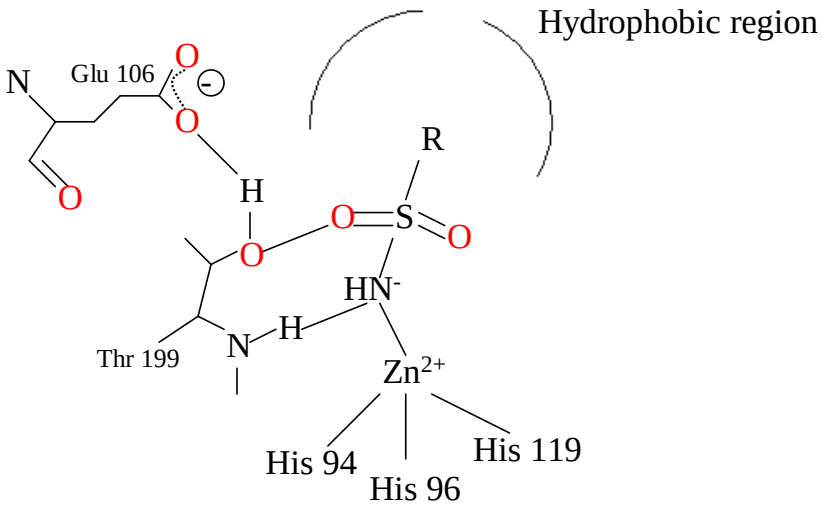

Figure 1-11. Diagram of sulfonamide binding to active site of CA II. [Adapted from Supuran *et al.*, 2004. Carbonic anhydrase: its inhibitors and activators. (Page 7, Figure 1.4) CRC Press, Boca Raton, Florida.]

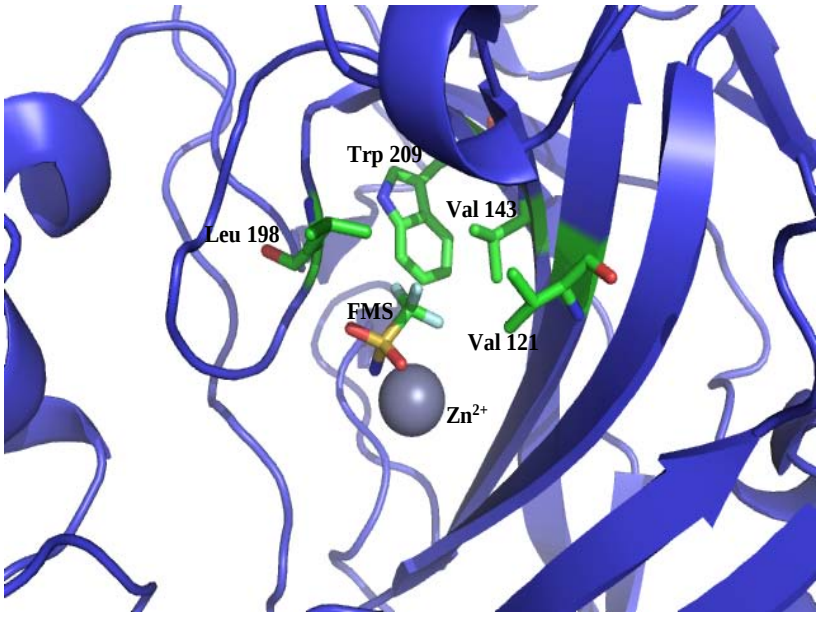

Figure 1-12. Crystal structure of human CAII complexed with trifluoromethane sulphonamide. The Zn^{2+} atom is labeled and shown as a gray sphere; side chain residues are labeled and atom coloring is depicted as follows: carbon (green), oxygen (red), nitrogen (blue), sulfur (orange), and fluorine (aquamarine). The trifluoromethyl group is shown interacting within the hydrophobic pocket of the active site. Ribbons and arrows convey helices and β-strands, respectively. The figure was generated in PyMol (DeLano, 2002).

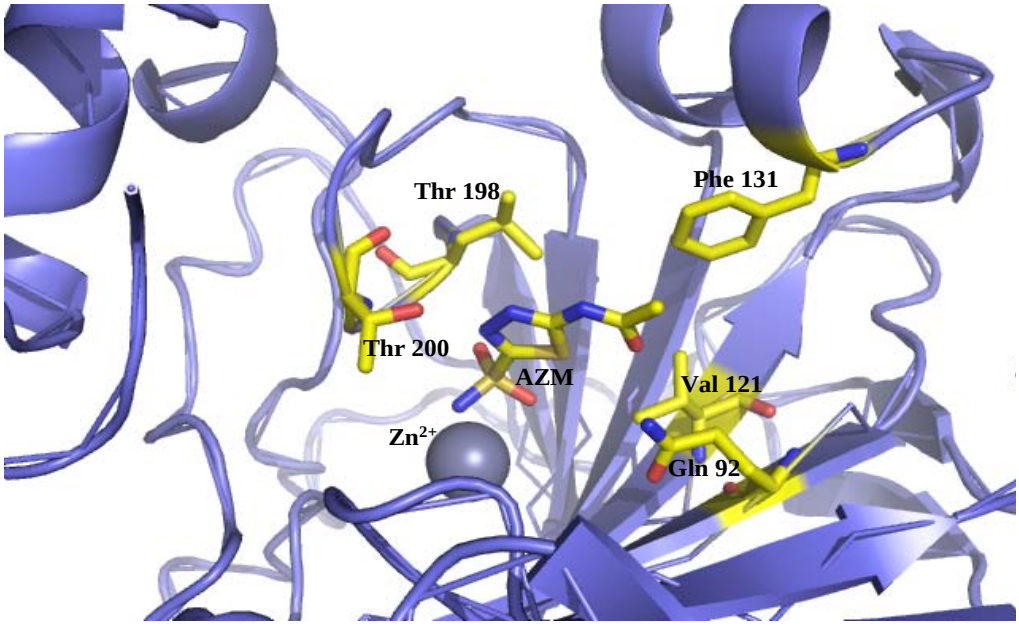

Figure 1-13. Crystal structure of human CA II complexed with acetazolamide. Zn^{2+} atom is shown as a gray sphere. Side chain residues are labeled and atom coloring is as follows: carbon (yellow), oxygen (red), nitrogen (blue), sulfur (orange). Figure was generated in PyMOL(DeLano, 2002).

Table 1-1. Apparent Affinity Constants of Anionic Inhibitors for hCA II

Anion	pK_{app} = -Log K_{app} hCA II
HO^-	-
HS^-	-
F^-	-
Cl^-	1.17
Br^-	1.57
I^-	2.51
Cl^-	-
CNO^-	-
SCN^-	3.09
N_3^-	-
HCO_3^-	-
HSO_3^-	-
NO_3^-	1.74
ClO_4^-	2.82
$HCOO^-$	1.74
CH_3COO^-	1.47
FCH_2COO^-	0.89
F_2CHCOO^-	1.30
F_3CCOO^-	1.96
$C_2O_4^{2-}$	1.74

[Adapted from Bertini, 1981. *Journal of the American Chemical Society* **103**, 7784-7788; Bertini, I. et al. (1978a) *Journal of the American Chemical Society* **100**, 4873-4877; Bertini, I. et al. (1982) *Structure and bonding* **48,** 45-92;Supuran, C.T., and Manole, G. (1999) *The Carbonic Anhydrase Inhibitors: Synthesis, Reactions and Therapeutical Applications*, Romanian Academy Publishing House, Bucharest.]

CHAPTER 2
CRYSTALLIZATION AND STRUCTURAL ANALYSIS OF CA II AND CA IX MIMIC COMPLEXED WITH ALTHIAZIDE

Introduction

X-ray crystallography has proven to be an effective tool for obtaining three-dimensional models for structural analysis. The primary limiting factor in X-ray crystallography, however, is the quality of the crystals. Protein crystals have a high solvent content which is about 30-80% as opposed to small-molecule organic or inorganic crystals which are held firmly together by ionic or covalent forces (Danley, 2006). The size and configuration of channels spanning the crystal is determined by the network of lattice interactions which is approximately 20 to 100 Å in diameter (Vilenchik, 1998). Because of the large solvent shells between protein molecules, only weak hydrophobic or hydrogen-bonding forces secure the molecules together in the crystal lattice. Consequently, highly ordered crystals can be difficult to obtain for high-resolution X-ray diffraction. X-ray radiation can also damage protein crystals and cause ions and radicals to form and diffuse throughout the solvent channels. However, these large solvent channels permit ligands, cofactors, and small molecules to traverse the channels in the crystals and form connections with the protein for structural study (Danley, 2006).

Structural information of inhibitors in adducts with their macromolecular targets can be determined at a molecular level and are used iteratively to develop new drugs. Binding occurs when free ligand (L) is added to its protein receptor (P); an equilibrium is subsequently formed between the protein, the ligand, and the ligand-protein complex (PL). The dissociation constant, Kd, can be described by Equation 2-1 (Danley, 2006):

$$Kd = [P][L]/[PL] \quad (2\text{-}1)$$

The fractional saturation Y is the amount of protein bound with ligand divided by the total protein and can be described by Equation 2-2:

$$Y = [PL]/[P] + [PL] \quad (2\text{-}2)$$

The equation for Kd can be substituted and be re-expressed as Equation 2-3:

$$Y = [L]/ Kd + [L] \quad (2\text{-}3)$$

This demonstrates how the ratio of [L] to Kd affects the fraction of protein in the ligand-bound form, Y. This ratio of these factors at equilibrium will be affected by the affinity and concentration of ligand added; this includes the ligand solubility as well. In order to achieve 90% occupancy, the amount of ligand added needs to be greater than the amount of protein so that at equilibrium, the free ligand [L] is not diminished to less than 10 x Kd (Danley, 2006). In order for the ligand to have crystallographic occupancy in the protein target, the ligand concentration ought to be tens of millimolar higher (Verdonk *et al.*, 2005, Nienaber *et al.*, 2000).

The duration times for complete ligand occupancy within a protein can vary from minutes to hours or even days. The causes for the prolonged time requirement to attain full occupancy are still under investigation, but some explanations have been proposed. Wu et al advanced the notion that at least 25-30% of the binding sites may need to be filled before electron density surrounding the ligand in the electron-density maps is visible (Wu, 2002). Upon soaking the crystal, this level of occupancy must take place from the surface towards the viscera of the crystal and may thus need longer times depending on the makeup of the bulk-solvent channels traversing the crystal lattice. In a crystal-soaking experiment, diffusion is predominantly impelled by the ligand-concentration gradient from the surface to the interior of the crystal (McNae, 2005). Studies on cross-linked protein crystals indicated that, in addition to the channel size, the chemical nature of the crystal can also influence the disjunction of molecules. The ligand may interact via polar or hydrophobic bonds and possibly size-exclusion

means in the channels and consequently, diffusion may be slowed down as the ligand attaches to the protein adduct (Danley, 2006).

Currently, therapeutic CA inhibitors have been designed on the basis of sulfonamide, sulfamate, and hydroxamate functional groups that coordinate the active site zinc ion (Supuran *et al.*, 2004). The objective of this experiment was to determine at the molecular level if a particular drug bound to the active site. The protein-ligand crystal structure was then solved and the drug-binding mechanism was accessed.

Materials and Methods

Expression and Purification

CA II and CA IX mimic were expressed by transforming the plasmid into Escherichia coli BL21(DE3)pLysS cells. The proteins were subsequently purified using an affinity resin p-aminobenzenesulfonamide (pAMBS) secured with agarose beads, which binds specifically to the active site of α-CAs (McPherson, 1982). Fractions of protein were collected and buffer exchanged into storage buffer (50mM Tris-HCl, pH7.8) using an Amicon Ultra-15 centrifugal filter device with a 10,000 molecular weight cutoff, concentrated, and assessed for expression and purity using a Coomassie-stained SDS-PAGE. The protein was concentrated to ~20 mg mL -1 as determined by measuring the optical density at 280 nm using a molar absorptivity of 5.5 x 104 M^{-1} cm^{-1}.

Crystallization

CA II and CA IX mimic crystals were grown at room temperature and obtained using the hanging-drop vapor-diffusion method (McPherson, 1982). The reservoir solutions contained a mixture of sodium citrate (1.3 M) and 100 mM of Tris-HCl at a pH of 9.0. Each CA II drop had a 6:4 ratio of protein (at ~20 mg mL-1 in 50 mM Tris-HCl, pH 7.8) to precipitant solution for a total volume of 10 µl. CA IX mimic crystallization drops were obtained by mixing 7µL protein

(at ~15 mg mL-1 in 50 mM Tris-HCl, pH 7.8), 3 μL of precipitant, and 1 μL of Hampton HR2-410-02 detergent (Hampton Research, Aliso Viejo, CA). The drops were pendent over 1 mL reservoir solution. Crystals were visible within 7 days.

Crystal Soaking

Althiazide was solubilized in 50% DMSO and water. Crystals of CA II and CA IX mimic were soaked with 4 mM althiazide for 24 hours prior to data collection.

Diffraction Data Collection

X-ray diffraction data for the CA II and CA IX mimic were collected on an in-house R-AXIS IV^{++} image plate system with a Rigaku generator, using a Cu K_α wavelength (1.5418 Å) (Osmic mirrors and a Rigaku RU-HU-H3R Cu rotating anode). Images were obtained using a crystal-to-detector distance of 80.0 mm using a 1° oscillation angle with an exposure time of 8 min per image. Overall there were 360 ° of frames collected for both crystals. There were a total of 37,503 reflections measured to a maximum resolution of 1.5 Å for the CA II crystal and 31,214 reflections measured to a maximum resolution of 1.6 Å for the CA IX mimic crystal. Both crystals belong to the $P2_1$ space group. CA II and CA IX mimic crystal had unit cell parameters of *a*=42.9 Å, *b*=41.9 Å, *c*=72.8 Å, and β=104.5˚ and *a*=42.9 Å, *b*=41.9 Å, *c*=72.8, and β=104.4˚ respectively. A set of 3532 (92.8% complete) and 2935 (93.6% complete) independent reflections for CA II and CA IX mimic, respectively, were collected. The data was indexed using *DENZO* and scaled with *SCALEPACK* using HKL2000 (Otwinowski, 1997).CA II had an R_{symm}=0.09 while CA IX mimic had an R_{symm}=0.015. The data collection statistics are given in Table 2-1.

Phasing, Model Building, Refinement Protocol

All the crystal structures were phased with the molecular replacement method using the software packages, Crystallography and NMR System (CNS) (Brunger, 1998). The phasing model used was obtained from the Protein Data Base, accession number 2ILI (Fisher *et al.*, 2007). The CA II and CA IX mimic structures complexed with althiazide were refined with the program SHELXL97 (Emsley & Cowtan, 2004, Sheldrick, 2008). The conjugate-gradient least-squares model (CGLS) with SHELXL default restrains were applied for the protein geometric parameters. During the refinement processes, the PRODRG server was used to produce the topology files for modeling the inhibitor structures (Schuttelkopf & van Aalten, 2004). The structures were manually modeled via the computer graphic program COOT (Emsley & Cowtan, 2004). Refinement of the structures ensued until convergence of Rcryst and Rfree was reached. The interactions between the inhibitor and enzyme were accessed by observing the environmental distances in COOT. Model geometries were subsequently determined using PROCHECK (Figure 2-1) (Emsley & Cowtan, 2004, Laskowski *et al.*, 1993). Table 2-2 shows the final model statistics (Figure 2-2).

Results and Discussion

While the refined crystal structures of CA II and CA IX clearly depicts althiazide bound within the active site of the enzyme, there is a lack of electron density surrounding the inhibitor's tail region in both structures (Figure 2-2) (Figure 2-3). This suggests that althiazide degraded in the enzyme and may thus be unstable.

The crystallographic parameters and refinement statistics for the hCA II-althiazide and CA IX mimic-althiazide complex are displayed in Table 2-1 and Table 2-2.. Figure 2-2 and 2-3 depict the omit map of the compound bound within both enzyme's active site. The crystal structures of the hCA II-althiazide complex and CA IX mimic-althiazide complex were isomorphous with the native protein. The crystal structures were thus solved by difference

Fourier techniques. Table 2-2 shows that the refined structures had good geometry with rmsd from ideal bond lengths of 0.0925 and 0.005, respectively for CA II and CA IX mimic, respectively**.** The quality of the model was good with all the residues in the allowed regions of the Ramachandran plot (Figure 2-1).

Figure 2-4 and 2-5 depict the interactions with amino acid residues present in both the hCA II and CA IX mimic active site in which the inhibitor participates, respectively. Althiazide typifies the sulfonamide binding mode where the ionized nitrogen group (N1) replaces the zinc-bound water molecule and is directly coordinated to the Zn(II) ion with the tetrahedral geometry maintained. This NH moiety hydrogen bonds to the hydroxyl group of Thr 199 while O2 of the SO_2NH group hydrogen bonds to the NH moiety of Thr 199. His 94 and Val 121 coordinate the aromatic ring via Van der Waals interactions. Table 2-3 displays the inhibitor-protein interactions.

Conclusions

While the electron density maps depict althiazide bound within the active site of CA II and CA IX mimic, the lack of electron density surrounding the inhibitor's tail region pose some interesting questions regarding the compound's structural stability and chemical interactions with the enzyme's amino acid residues. A hydrogen located on C5 may have been abstracted by the enzyme's amino acid residues, ultimately leading to the elimination of the inhibitor's tail. Analysis of the inhibitor's chemical interactions and bond distances indicate that the tetra-coordinated geometry is still preserved. Althiazide appears to be stabilized by a hydrogen bonding network that is mediated by residues Thr 199 and Glu 106. Van der Waals interactions also contribute to the inhibitor's binding. Althiazide's chlorobenzenesulfonamide moiety coupled with the planarity of the aromatic ring may account for the inhibitor's binding to the active site. The binding of althiazide seems to have generated a shift in the position of the active

site water molecules. Consequently, there are no water molecules that participate in hydrogen bonds with the inhibitor.

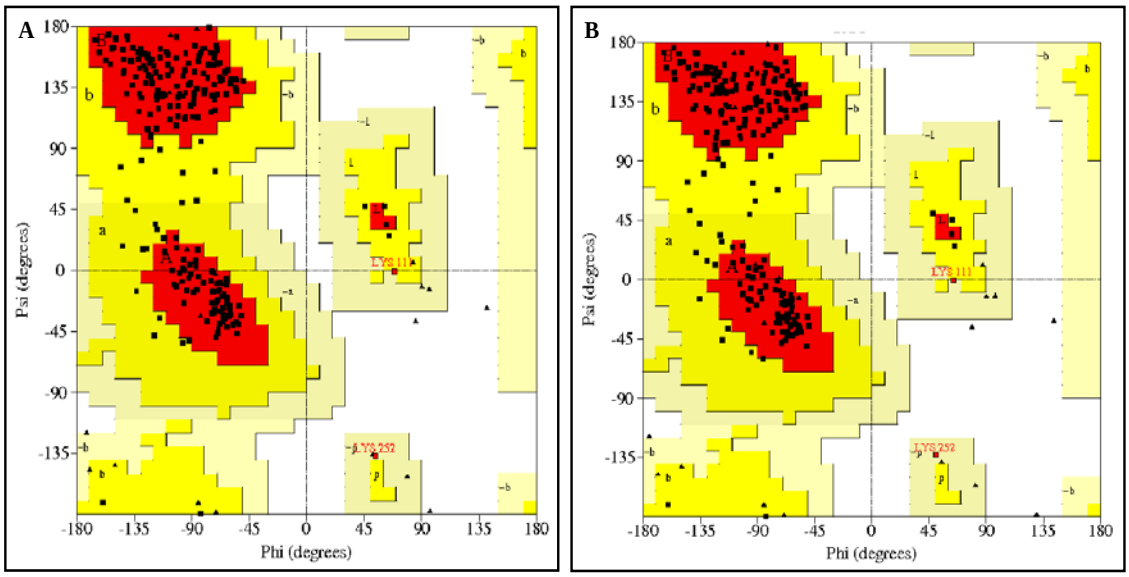

Figure 2-1. Ramachandran diagram for wild-type human CA II A) and CA IX mimic B) complexed with althiazide. Plot created using Procheck (Laskowski et al., 1993).

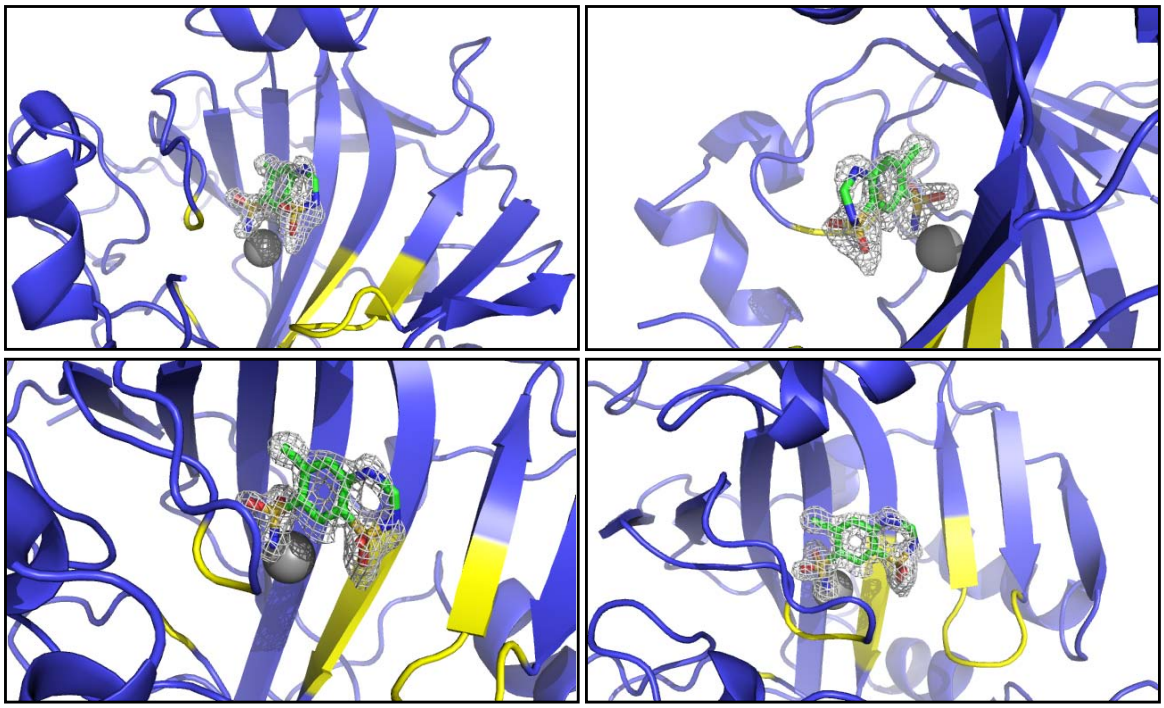

Figure 2-2. Four different views of the crystal structure of human CA II complexed with althiazide. The Zn^{2+} atom is shown as a gray sphere. Ribbons and arrows convey helices and β-strands, respectively. The yellow depicts the active site residues. The gray 2Fo-Fc electron density map is contoured at 1.5σ. The figures were generated in PyMol (DeLano, 2002).

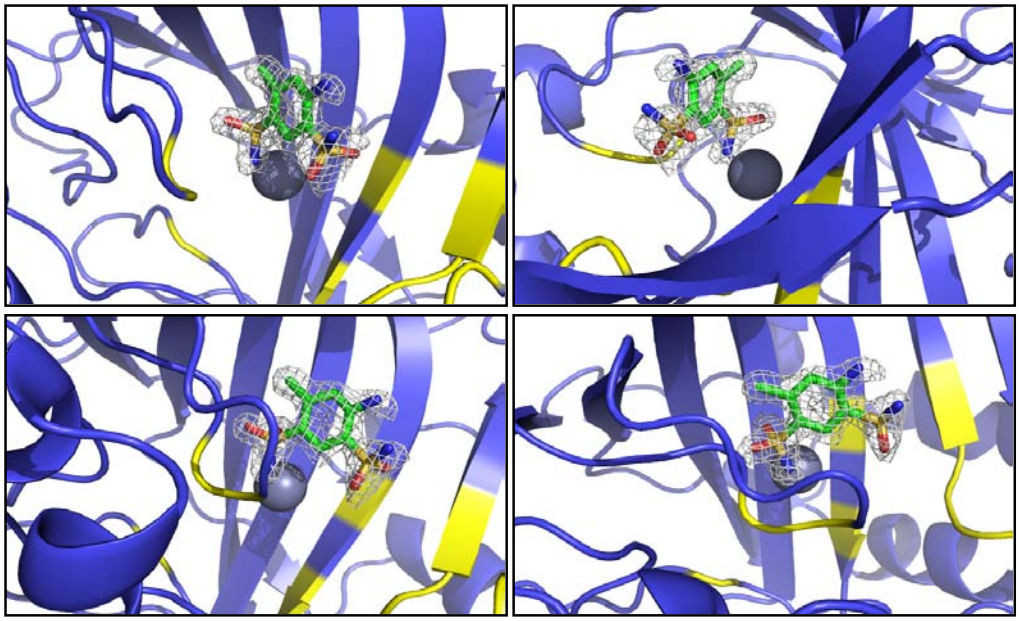

Figure 2-3. Four different views of the crystal structure of human CA IX mimic complexed with althiazide. The Zn^{2+} atom is shown as a gray sphere. Ribbons and arrows convey helices and β-strands, respectively. The yellow depicts the active site residues. The gray 2Fo-Fc electron density map is contoured at 1.5 σ. The figures were generated in PyMol (DeLano, 2002).

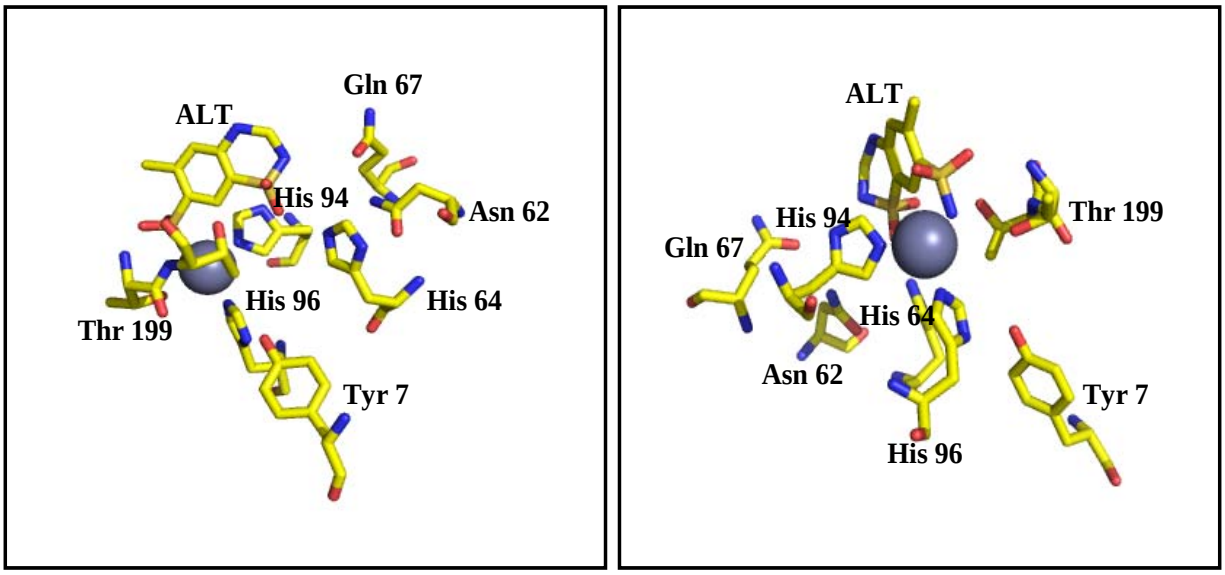

Figure 2-4. Crystal structure of the active site of CA II in complex with althiazide. Zn^{2+} atom is shown as a gray sphere. Side chain residues are labeled and atom coloring is as follows: carbon (yellow), oxygen (red), nitrogen (blue), sulfur (orange). Figures were generated in PyMol (DeLano, 2002).

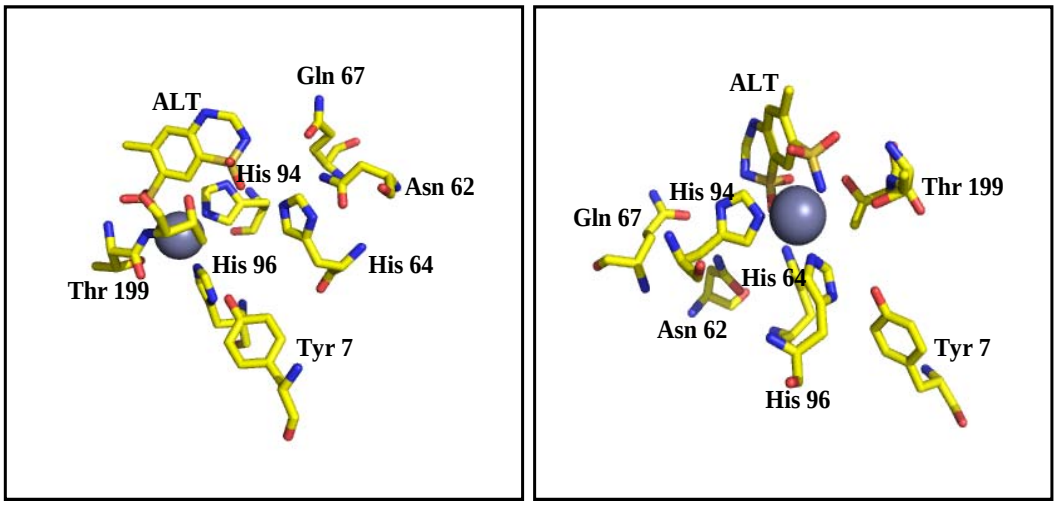

Figure 2-5. Crystal structure of the active site of CA IX mimic in complex with althiazide. Zn^{2+} atom is shown as a gray sphere. Side chain residues are labeled and atom coloring is as follows: carbon (yellow), oxygen (red), nitrogen (blue), sulfur (orange). Figures were generated in PyMol (DeLano, 2002).

Table 2-1. X-ray Crystallographic Data Collection Statistics for CA II and CA IX Mimic Complexed with Althiazide

Data Set Statistics	CA II-Althiazide	CA IX Mimic-Althiazide
Space Group	$P2_1$	$P2_1$
Unit-cell parameters (Å,°)	a=42.9	a=42.9
	b=41.9	b=41.9
	c=72.8	c=72.8
	β=104.5	β=104.4
Resolution (Å)	50-1.5	50-1.6
	(1.55-1.5)	(1.66-1.6)
Total number unique reflections	37503 (3532)	31214 (2935)
Redundancy	4.4	1.1
Completeness (%)	92.8 (87.9)	93.6 (88.4)
R_{symm}[a]	0.09	0.015

[a] $R_{symm} = \Sigma |I - \langle I \rangle| / \Sigma \langle I \rangle$.

Table 2-2. X-ray Crystallographic Refinement Statistics for CA II and CA IX Mimic Complexed with Althiazide

Model Statistics	CA II-Althiazide	CA IX Mimic-Althiazide
[a]R_{cryst}	0.156	0.1622
[b]R_{free}	0.170	0.206
Rmsd for bond lengths (Å)	0.093	0.005
Average B-Factors (Å^2)		
Main/side/solvent/drug	17.8/24.4/36.2/21.5	18.2/25.0/43.3/20.7
Ramachandran Statistics (%)		
Preferred/Allowed/ Outliers	92.9/7.1/0	93.7/6.3/0
No. protein atoms	261	261
No. water molecules	180	205

[a] $R_{cryst} = \Sigma |F_o| - |F_c|/\Sigma |F_{obs}| \times 100$. [b] R_{free} is calculated in the same fashion as R_{cryst}, except that it uses 5% of the reflection data omitted from refinement.

Table 2-3. Protein-Inhibitor Interactions

Althiazide	wt hCA II residue	Distance (Å)
N1	Zn	2.01
O1	Zn	3.04
N1	Oγ1Thr199	2.80
O2	Oγ1Thr199	3.70
O2	NThr199	2.95
O1	Nδ1His119	3.39
O3	Oγ1Thr200	3.15
CL1	Cγ2Val143	3.44
C6	Cε1His94	3.39
C3	Cγ2Val121	4.14
Althiazide	**CA IX Mimic residue**	**Distance (Å)**
N1	Zn	1.99
O1	Zn	3.04
N1	Oγ1Thr199	2.85
O2	Oγ1Thr199	3.73
O2	NThr199	2.97
O1	Nδ1His119	3.44
O4	Oγ1Thr200	3.23
CL1	Cγ2Val143	3.47
C6	Cε1His94	3.39
C3	Cγ2Val121	4.04

CHAPTER 3
STRUCTURAL VALIDATION OF ALTHIAZIDE VIA NMR SPECTROSCOPY

Introduction

NMR spectroscopy has become a powerful and effective tool for the structural determination of biomolecules at atomic resolution. In addition to providing the conformational information of a molecule, NMR is also used for determining the direct hydrogen bonding interactions and serves as a means for analyzing a compound's motional properties as well.

Various complementary pieces of information can be extracted from a 1D 1H NMR spectrum. The chemical shift elucidates the dependence of nuclear magnetic energy levels on a molecule's electronic environment (Ernst, 1987). An atomic nucleus can have a magnetic moment which yields various energy levels and resonance frequencies in a magnetic field. The total magnetic field that a nucleus experiences is comprised of local magnetic fields which are induced by electron currents in the molecular orbits (Akitt, 1983). Binding partners, bond lengths, and angles between bonds affect the electron distribution of the nucleus and the local magnetic field. This is observed in the spin energy levels and resonance frequencies (Akitt, 1983). The chemical shift can thus be described by the variations of nuclear magnetic resonance frequencies of the same type of nucleus as a result of the fluctuations in the electron distribution. The electrons surrounding a nucleus will move in a magnetic field and produce a secondary induced magnetic field. Lenz's law proclaims that this field opposes the applied field and the nucleus is consequently shielded (Ernst, 1987). The degree of shielding or deshielding can account for the trends in chemical shift. In real molecules, however, a cloud of charge caused by adjacent bonds and atoms surround the protons. Electrons in an applied magnetic field (B_0) generate an induced field (B_i) which counters the applied field. The effective field at the nucleus is thus represented by Equation 3-1:

$$B = B_0 - B_i \quad (3\text{-}1)$$

The nucleus is now undergoing diamagnetic shielding. The electron density, electronegativity of neighboring groups, and the anisotropic induced magnetic field effects are all important factors that affect the chemical shift (Ernst, 1987).

The spin coupling information yields information regarding the amount of proximate protons. Nuclei that experience the same chemical shift are referred to as equivalent; alternatively, nuclei that experience a different chemical shift are called nonequivalent. Nuclei that are adjacent to one another induce an effect on each other's magnetic field and thus, when the nuclei are nonequivalent, these effects can be observed in the NMR spectrum (Ernst, 1987). The effect is evident when the distance between nonequivalent nuclei is less than or equal to three bond lengths. This effect is termed J-coupling.

The intensity data reveals the relative numbers of each type of proton. While the intensities can sometimes be obtained by inspection, the area of each peak may serve as a better guide because lines have different breadths. Spectrometers are equipped with an integrating device which determines the number of protons.

Two-dimensional correlation spectroscopy (COSY) has many broad applications in the studies of inter and intramolecular interactions, chemical reactions, electrochemistry, photochemistry, adsorption, hydration, denaturation, and more. It has become an increasingly advantageous technique because of its ability to simplify complex spectra that are comprised of many overlapping peaks and its ability to enhance spectral resolution via peak broadening over the second dimension (Noda, 2004). Through the correlation assignments of the bands, clear assignments can be established. However, this technique carries one major drawback. In order to effectively use the original data analysis scheme, the time-dependent behavior of dynamic

spectral intensity variations needs to be a simple sinusoid (Noda, 2004). This issue was rectified by Noda in 1993 who broadened the concept of 2D correlations spectroscopy to incorporate more general forms of spectroscopic application. The mathematical procedure that provided the 2D correlation spectra from sinusoidally changing time-dependent spectral signals was adjusted to tackle arbitrary time-dependencies (Noda, 2004).

2D spectra are produced from a set of continuous spectral data from a particular sample that is affected by a specific external disturbance that instigates selective changes in the features of the spectra. A diverse array of physical origins (i.e. thermal, mechanical, optical, or chemical) and waveforms (i.e. sinusoid, pulse, ramp) can be used for the external disturbance (Ozaki, 2001). Different chemical components of the system become excited when the system is externally disturbed. Electromagnetic probes survey the excitation and subsequent relaxation towards equilibrium. A set of dynamic spectra must first be calculated prior to the construction of generalized 2D correlation spectra. Synchronous and asynchronous spectra are then created from the dynamic spectra.

Heteronuclear Multiple-Quantum Coherence is a technique that establishes correlations between nuclei such as 13C or 15N in proteins, with 1H resonances via the coherence or polarization between the heteronuclear (S) and 1H (I) spins. To have coherence transfer, the NMR experiment can begin with excitation of either I or S spin polarization and must end with the identification of either I or S spin magnetization (Cavanagh, 1996). In a general sense, the sensitivity of HMQC experiments can be described by Equation 3-2 (Cavanagh, 1996):

$$S/N \alpha \gamma ex(\gamma det)3/2 [I - exp(-RlexT)], \quad (3\text{-}2)$$

where γex and γdet are the magnetogyric ratios of each nucleus excited at the onset of the sequence and detected at the end of the sequence, respectively, T is the experiment's recycle

time, and Rlex is the spin-lattice relaxation rate constant of the excited nucleus. In order to maximize the sensitivity, proton detection is used.

Heteronuclear Multiple Bond Correlation (HMBC) experiments detect long range coupling between a proton and a carbon that are separated by two, three, and occasionally four bonds with high sensitivity. Small coupling constants (2-7 Hz) $\tau = 0.1$ sec or larger couplings (4-10 Hz) $\tau = 0.06$ sec can be detected by modifying the length of the τ delay (Cavanagh, 1996). In contrast to HMQC, HMBC has a poorer sensitivity because of smaller J values involved and the interference of 1H-1H coupling (Cavanagh, 1996).

Many samples that are run on D_2O are obscured from residual H_2O signal causing the actual small molecule signals to become overpowered. Unlike water which has a concentration of 55 M, small molecules typically have a concentration of ~100 μM and thus, any residual protons which have exchanged with the D_2O will overwhelm any small molecule signal that does not have an adequate concentration (Furihata, 2007). To overcome this issue, there are water suppression methods that use a low power pulse at the solvent frequency and are applied during the preparation delay. The water proton signal becomes excited by the low power pulse such that no signal can completely accumulate and be detected (Furihata, 2007). When there is a need to suppress large solvent signals, water suppression by presaturation is used. However, this method has some drawbacks which include a possible saturation transfer to exchangeable NH protons, the bleaching of signals near water, and the formation of a large dispersive tail from the water signal. The WATERGATE experiment is another means of suppressing the water signal (Wu, 2003). This method uses a strong Z-gradient pulse to destroy transverse magnetization. Another z-gradient pulse of the same amplitude but of opposite phase can be applied to refocus a destroyed or dephased magnetization. The two additional selective 90 ° pulse on water allows

the second z-gradient pulse to act as another defocus gradient pulse. The second Z-gradient can also act as a refocus gradient via the 180 ° pulse (Wu, 2003).

Crystallographic studies indicate that althiazide binds within the CA II and CA IX mimic active site. However, a lack of electron density surrounding the tail of althiazide suggests that the compound may be degrading within the enzyme and may thus be unstable. The possibility that the drug may degrade to a toxic substance or lose its potency makes it necessary to investigate. The causes of althiazide's instability may occur via two parallel pH-sensitive pathways or may be a result of the chemical reactivity within the active site of carbonic anhydrase. Thus, several experiments were performed via 1D 1H NMR, 2D HSQC, HMBC, and COSY in an attempt to determine the cause of althiazide's aberrant behavior within the enzyme.

Preparation of pH Adjusted Althiazide Samples

Alkaline and acidic solutions of althiazide were prepared in order to assess the pH dependent changes in the compound's structure. Three samples (designated A, B, and C) contained 10 mg/0.75 mL of althiazide and were solubilized in 50% D2O and 50% DMSO-D6. Sample A had no pH modifications and served as a control. NaOH was added to sample B, bringing the pH to ~11. Sample C was acidified via the addition of HCl, bringing the pH to ~ 1-2. The samples were left standing for 24 hours prior to testing.

1D ^{1}H NMR, 2D COSY, and ^{1}H/^{13}C HSQC/HMBC Studies

All 1D and 2D NMR spectra were acquired at 24° C with standard techniques using TopSpin software. Experiments were conducted on a Bruker Avance II 600 spectrometer equipped with a 5 mm TXI CryoProbe. Various pH-adjusted solutions of althiazide (~10 mg/0.75 mL) in 50% D2O/50% DMSO-D6 were assessed in 5 mm NMR tubes. ^{1}H-DMSO-D_5 served as the ^{1}H chemical shift internal reference, assigned to 2.5 ppm, and the corresponding ^{13}C signal was assigned to 39.5 ppm (Gottlieb, 1997). Proton spectra were taken with a 10 ppm

spectral width (SW) at 600.23 MHz using a 30° pulse, a 2.72 sec acquisition time and a relaxation delay of 0.1 sec. The ^{1}H spectra were phased via the command "apks" and baseline corrected prior to integration. The COSY data sets were acquired with Bruker's "cosygpqf" pulse sequence using an SW of 10 ppm in both dimensions. Eight scans were run for HSQC experiments; the data sets were run with Bruker's "hsqcedetgpsisp2.2" pulse sequence. Additional HSQC spectral parameters were as follows: ^{13}C spectrometer frequency (SF) 150.94 MHz, acquisition time (AQ) 0.14 sec, ^{13}C SW 170 ppm, and 256 increments in the indirect dimension. HMBC experiments were run with 12 scans. The data sets were acquired with Bruker's "hmbcetgpnd" pulse sequence. The spectral conditions remained the same with the exception of the acquisition time which was 0.17 sec.

Results of pH Adjusted Althiazide Solutions

All chemical shifts reported in this section are listed in ppm, and coupling constants are reported only for the ABX pattern for H-4a, H-4b, and H-5 in Hz. The ^{1}H NMR spectra for the neutral sample (A) was typical of the althiazide structure displaying aromatic proton signals at 7.97 and 6.99, vinyl hydrogen peaks at 5.71, 5.08, and 5.05, and aliphatic hydrogens at 4.82, 3.15, 2.83 and 2.76 (Figure 3-1A). The coupling constants for the significant ABX pattern (2.83, 2.76, and 4.82 ppm) in sample A are: J-H-4a, H-4b=14.1, J-H4a, 5=7.4, and J-H4b, 5=5.5. The HSQC and HMBC experiments displayed H-7 and H-6 coupled to C-A and C-B respectively. H-2 was situated at C-C, H-1a and H-1b with C-D, and H-5 with C-E. H-3 was positioned at C-F and H-4a and H-4b were positioned at C-G (Figure 3-2). Some of the chemical shifts in the ^{1}H NMR spectrum for the alkaline sample (B) were moderately different from those of sample A (aromatic protons 7.78 and 6.68, vinyl hydrogens 5.71, 5.07, and 5.03, and aliphatic hydrogens 4.71, 3.09, 2.72 and 2.56), but the general coupling patterns remained the same (Figure 3-1) The chemical shifts in the ^{1}H NMR spectra for the acidic sample (C) were quite similar to those of

sample A (aromatics 7.97 and 7.00, vinyls 5.70, 5.07, and 5.04, and aliphatics 4.71, 3.14, 2.83 and 2.78) (Figure 3-1). Most importantly, the ^{1}H NMR spectra for all samples displayed the distinctive ABX pattern between H-4a, H-4b, and H-5, indicating that the bond between C4 and C5 remain intact (Figure 3-3). These experiments indicate that general acid or base chemistry is not responsible for the anomaly observed in the X-ray crystal structure.

Conclusions

^{1}H NMR, HSQC, HMBC, and COSY experiments allowed the assignments of all proton and carbon signals. Since the ^{1}H NMR spectra for samples A, B, and C show no significant changes in the structure of althiazide, this indicates that it remains relatively stable under extreme variations in pH. Since althiazide is a clinically established diuretic that is intended for oral use, the compound must have already been tested to ensure that it maintained its stability under the pH conditions found in the gastrointestinal tract which may attribute to althiazide's stability under variable pH conditions.

Materials and Methods

Preparation of CA-exposed Althiazide

Since it was evident from the 1D ^{1}H NMR spectra that variations in althiazide's pH made no dramatic modifications to its structure, additional studies investigating the chemical effects of the enzyme on the inhibitor were performed. Four solutions (designated A1 and A2, B, C, and D1 and D2) of althiazide in storage buffer and varying molar ratio concentrations of althiazide to CA II were prepared. All samples of althiazide were solubilized in 50% DMSO-D_6. Sample A1 contained 50 mM althiazide and CA II storage buffer (50 mM Tris-HCl) in water. This sample was left standing for ~48 hours prior to testing. Sample A1 was prepared in order to determine whether or not althiazide had degraded in CA storage buffer alone. Sample B was prepared by aliquotting 5 μL of a 0.2 M althiazide solution and adding it to a 1 mL sample of CA II (~14.5

mg mL^{-1}) in storage buffer (50 mM Tris-HCl). Sample C was prepared by aliquotting 100 μL of a 900 nM althiazide solution and adding it to a 1 mL sample of CA II (~27.8 mg mL^{-1}) in storage buffer. The melting temperature of CA is 59 °C; thus after samples B and C were left standing for ~24 hours, they were submerged in a 70 °C water bath for 1 hour to denature the protein. B and C were subsequently filtered in a Millipore Microcon centrifugal filter device with a 10,000 molecular weight cutoff to remove the protein. SDS-PAGE analysis confirmed that no protein was present in samples B and C. Sample D contained 50 mM althiazide and phosphate buffer solution (PBS) at pH 7 and served as the control Sample A1 and D1 were later submerged in a 70 °C water bath for 1 hour to eliminate the possibility that a heat catalyzed hydrolysis caused the deterioration in althiazide's ring structure.

1D ^{1}H NMR Studies

All NMR spectra were acquired at 37° C with standard techniques using XWinNMR software on a Bruker Avance 500 spectrometer equipped with a 5 mm TXI probe. All samples were tested in a 5 mm NMR tubes (Norell, Inc.). The water signal was suppressed via a presaturation (zgpr) during a 2 sec relaxation delay or WATERGATE (Bruker sequence "p3919gp") sequence. Proton spectra were taken with a 10 ppm spectral width (SW) at 600.23 MHz using a 30° pulse, a 2.72 sec acquisition time and a relaxation delay of 0.1 sec.. The spectra were phased via the command "apks" and baseline corrected before integration. ^{1}H - DMSO-D_5 served as the ^{1}H chemical shift internal reference, assigned to 2.5 ppm (Gottlieb, 1997).

Results

All chemical shifts reported in this section are listed in ppm . The ^{1}H NMR spectrum for sample A1 (control) exhibited a spectrum similar to that of the neutral sample of althiazide in the

previously described pH experiment, including the significant ABX pattern for H-4a, H-4b, and H-5 (Figure 3-4). The ^{1}H spectrum for sample B (exposed to CA), however, implied markedly distinct changes in the compound's structure. After althiazide was incubated with carbonic anhydrase, the aromatic proton signals were shifted downfield at 8.12 and 6.98. Vinyl peaks were seen at 5.69 and 5.05. Evidence of a proton signal for H-5 was not obvious. It was not possible to unambiguously assign resonances to hydrogens 4a and 4b. In fact, they appeared to be missing (Figure 3-5); the ABX spin system that was manifest in sample A was absent in sample B. While the ^{1}H NMR spectrum for sample C showed similar proton signals as the spectrum for sample B, peaks for the vinyl regions of the compound were even more difficult to interpret. Again, after exposing althiazide to a smaller concentration of CA, aromatic proton signals were observed at 8.11 and 6.99. Vinyl peaks were seen at 5.71 and 5.0, but the proton signals for H-5, H-4a, and H-4b were not discernible; the aliphatic ABX spin system was also absent in sample C (Figure 3-6). The spectrum for sample D1 depicted the characteristic proton signals for althiazide, displaying aromatic proton signals at 7.99 and 7.0, aliphatic peaks at 4.85, 3.12, 2.82, and 2.75 and vinyl peaks at 5.75 and 5.12. The ABX pattern was also clearly observed (Figure 3-7). Applying heat to samples A1 and D1 did not significantly alter the proton signals as observed from the spectra for A2 and D2. While there were minor changes in the chemical shift for sample A2, the key peaks were still present, indicating that althiazide had remained relatively stable under heat conditions (Figure 3-8). Nevertheless, there were aromatic proton signals at 7.9 and 6.99, aliphatic resonances at 4.81, 3.19, 2.81, and 2.75, along with vinyl peaks at 5.72 and 5.12. Sample D2 also maintained the characteristic proton signals of althiazide, showing aromatic peaks at 8.1 and 6.98, aliphatic resonances at 4.86, 3.17, 2.82, and 2.79 and vinyl peaks at 5.75 and 5.12.

Conclusions

The chemical stability of a drug is dependent on intrinsic factors such as the compound's molecular structure and environmental factors such as temperature, pH, buffer species, ionic strength, light, oxygen, moisture, and excipients (Yoshioka, 2002). Subjecting althiazide to various conditions revealed some interesting information regarding the chemical nature and behavior of the compound. It was evident that althiazide maintained its structural integrity after prolonged exposure to CA storage buffer (50 mM Tris-HCl) and phosphate buffer solution and even subsequent heat treatment. However, after subjecting althiazide to varying concentrations of CA II, the data from this study suggests that the degraded compound may be a result of the chemical interactions that are occurring within the active site of the enzyme. Althiazide is susceptible to many different degradation pathways which may include hydrolysis, oxidation, elimination, or complex interactions with the enzyme's active site residues.

Hydrolysis of the compound can result in the opening of the ring or degradation of the side chain via chain scission (Hamid, 1992). The reactive nitrogen atoms that are adjacent to C-E also enhance the compound's susceptibility to hydrolysis which is then accompanied by the elimination of the vinyl tail region**.**

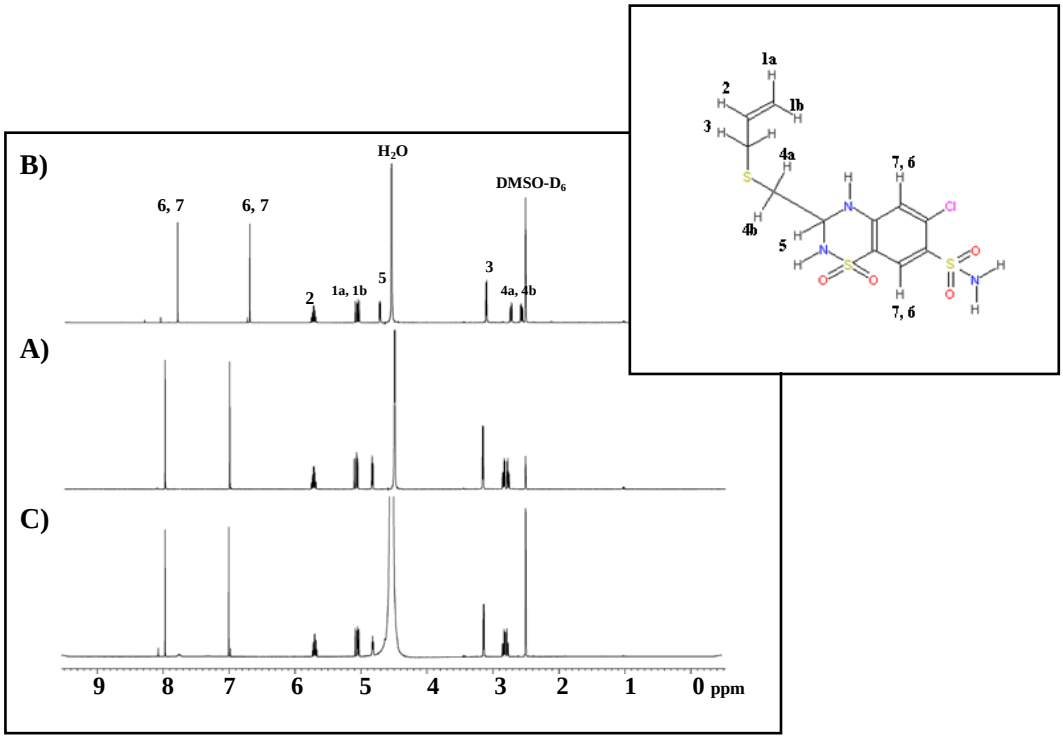

Figure 3-1. 1D 1H NMR spectra for pH Adjusted samples. A) Sample A (10 mg 0.75 mL-1, 50% D_2O/ 50% DMSO-D6) B) Sample B (10 mg 0.75 mL-1, 50% D2O/ 50% DMSO-D6, pH ~9) C) Sample C (10 mg 0.75 mL-1, 50% D2O/ 50% DMSO-D6 pH ~1-2). The rightmost panel is a key of the labeled hydrogens on althiazide.

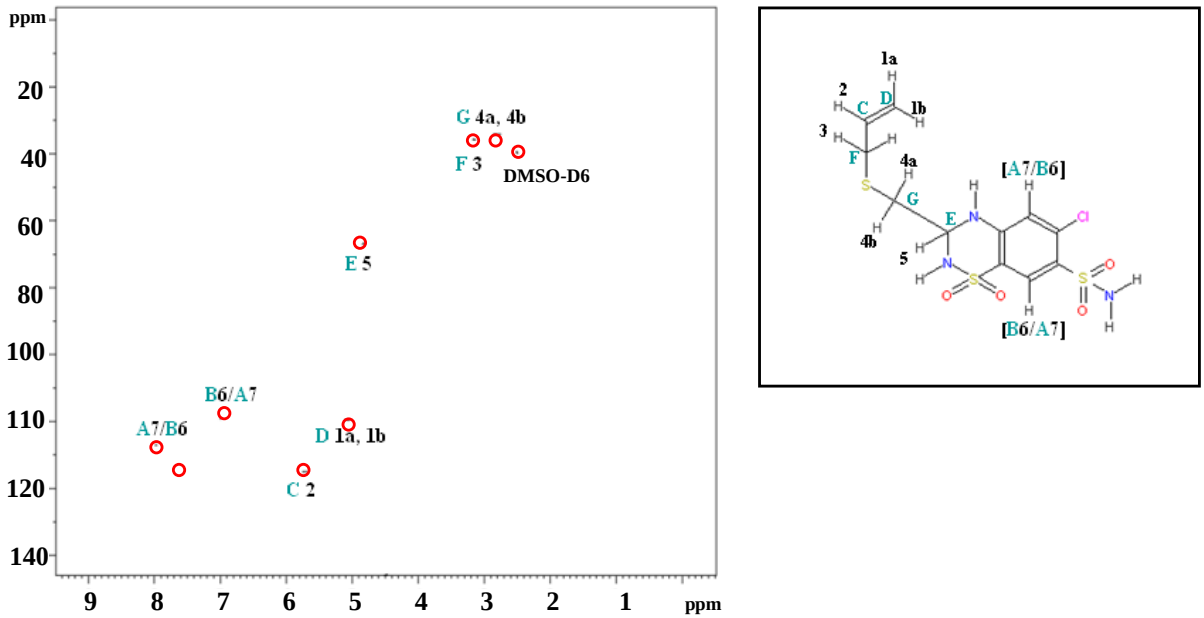

Figure 3-2. HSQC spectrum for sample A (10 mg 0.75 mL-1, 50% D2O/ 50% DMSO-D6) The rightmost panel is a key of the labeled hydrogens and carbons on althiazide..

.

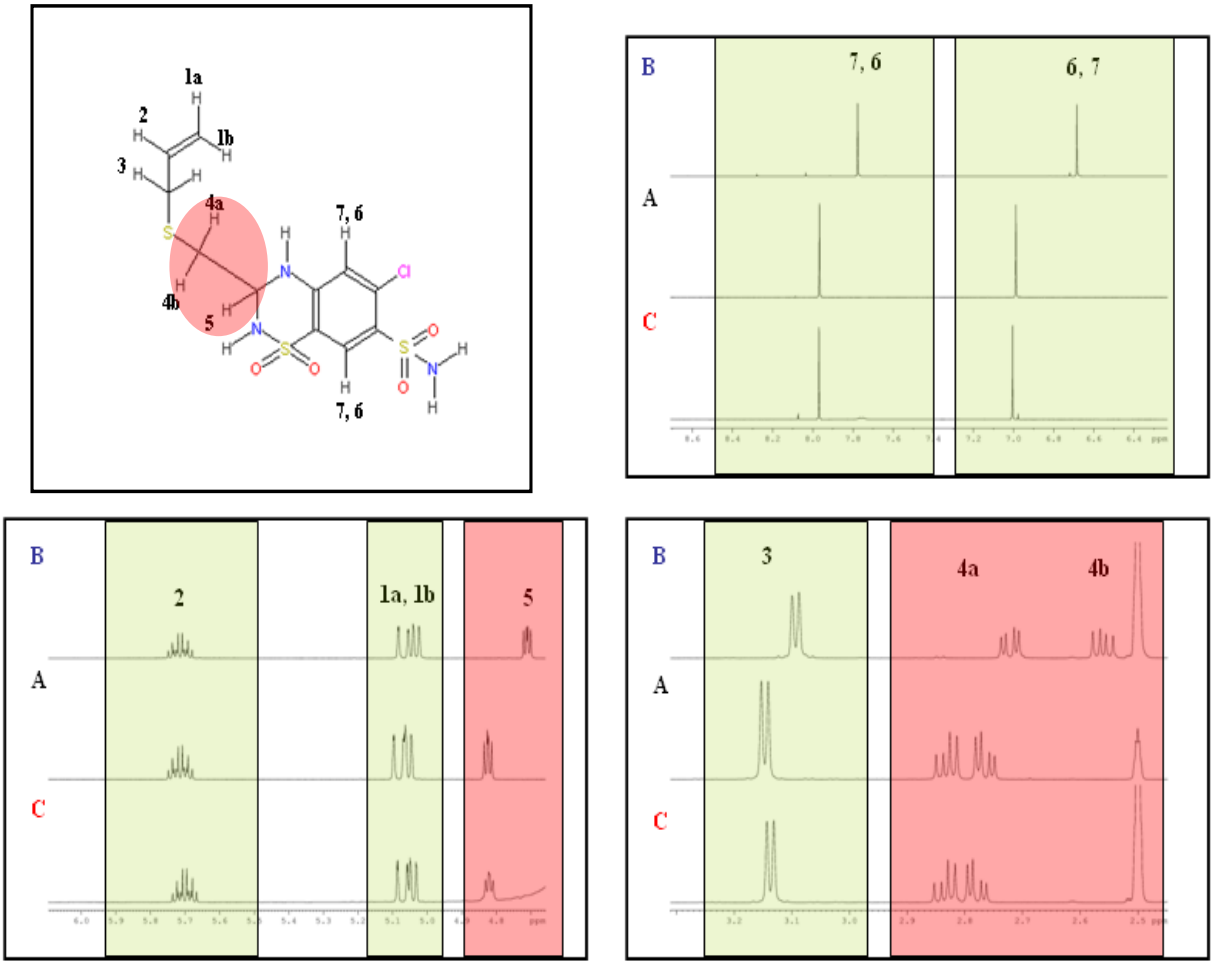

Figure 3-3. Magnified view of 1D 1H NMR spectra for pH Adjusted samples. A) Sample A (10 mg 0.75 mL-1, 50% D2O/ 50% DMSO-D6) B) Sample B (10 mg 0.75 mL-1, 50% D2O/ 50% DMSO-D6, pH ~9) C) Sample C (10 mg 0.75 mL-1, 50% D2O/ 50% DMSO-D6 pH ~1-2). Aromatic, aliphatic, and vinyl protons are highlighted in green. The significant ABX pattern is highlighted in red. The top leftmost panel is a key of the labeled hydrogens on althiazide.

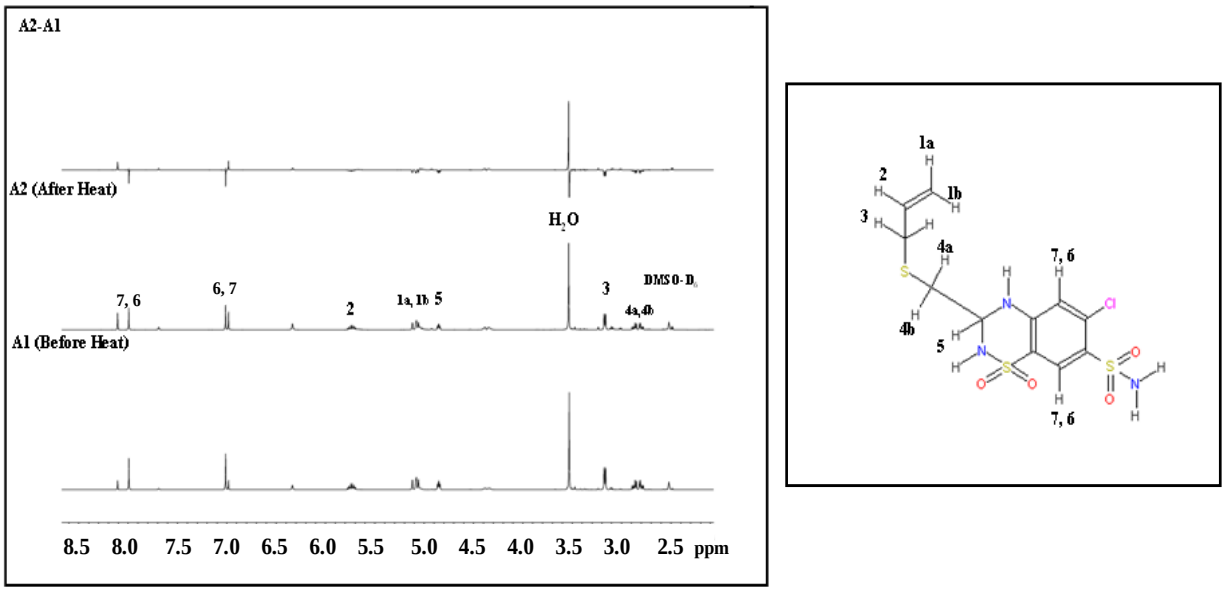

Figure 3-4. Comparison of 1D 1H NMR spectra for samples A1 and A2. The rightmost panel is a key of the labeled hydrogens on althiazide.

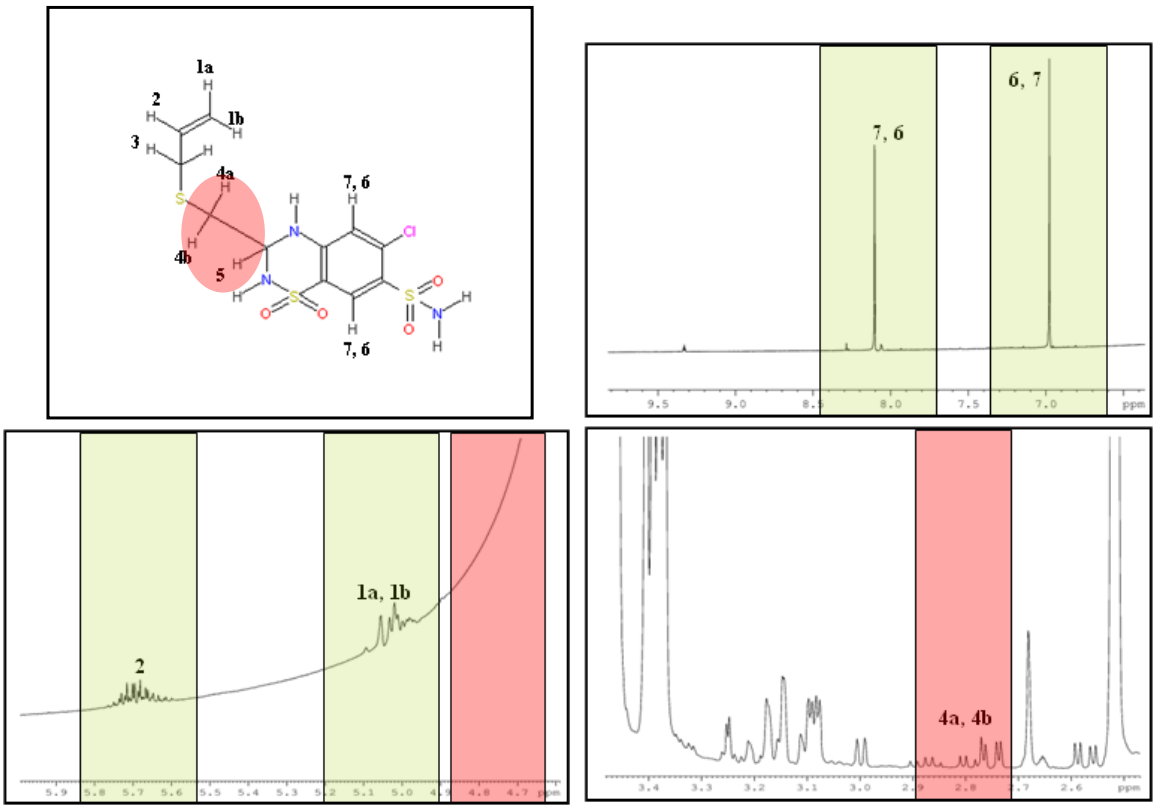

Figure 3-5. Magnified 1D 1H NMR spectrum for Sample B. Aromatic, aliphatic, and vinyl protons are highlighted in green. The significant ABX pattern is highlighted in red. The top leftmost panel is a key of the labeled hydrogens on althiazide.

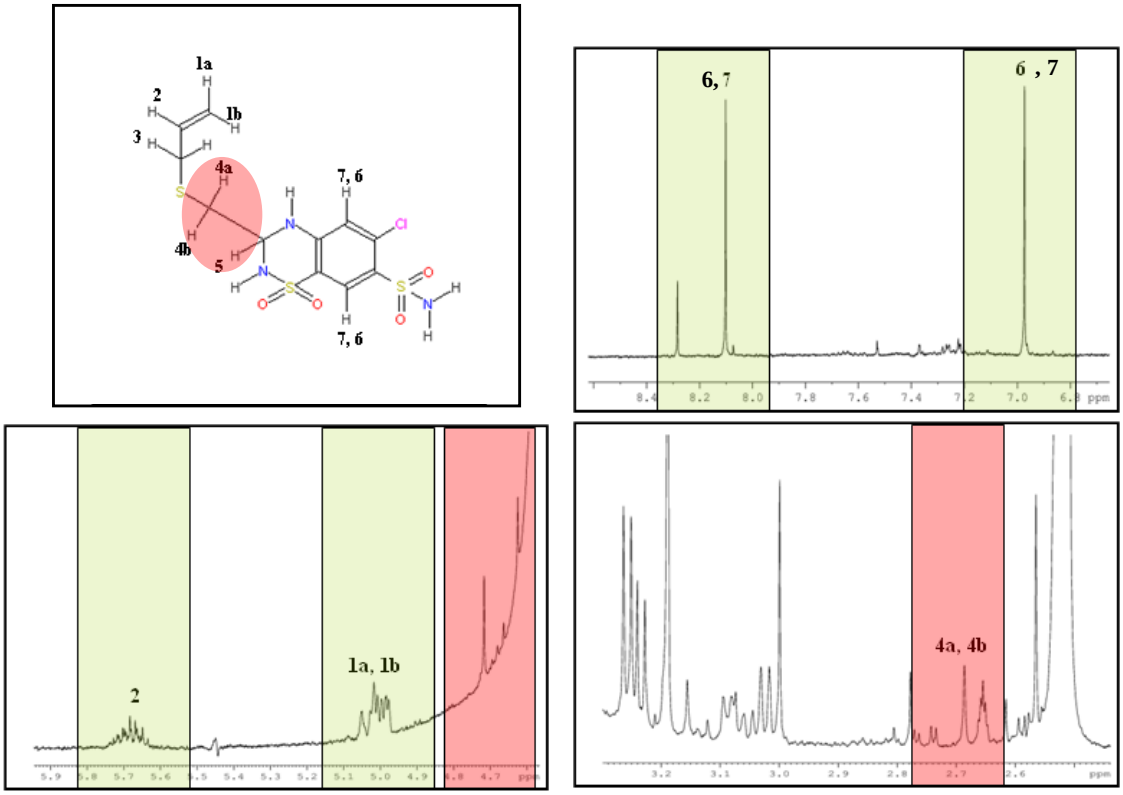

Figure 3-6. Magnified 1D 1H NMR spectrum for Sample C. Aromatic, aliphatic, and vinyl protons are highlighted in green. The significant ABX pattern is highlighted in red. The top leftmost panel is a key of the labeled hydrogens on althiazide.

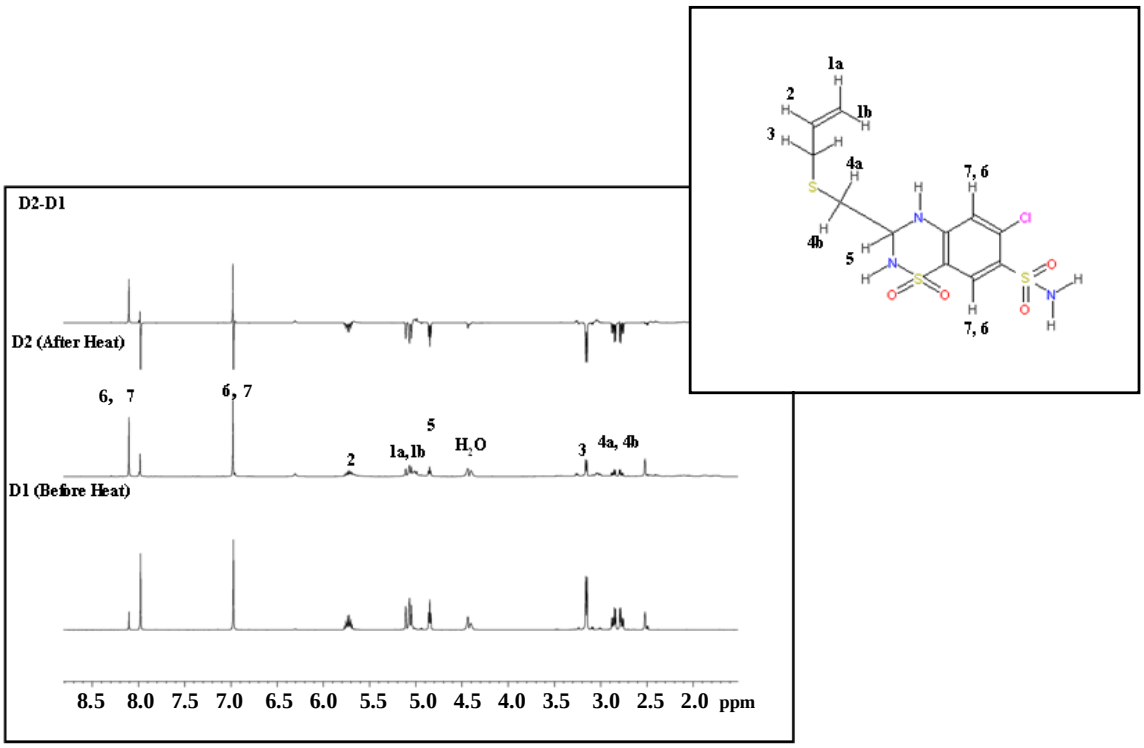

Figure 3-7. Comparison of 1D 1H NMR spectra for samples D1 and D2. The rightmost panel is a key of the labeled hydrogens on althiazide.

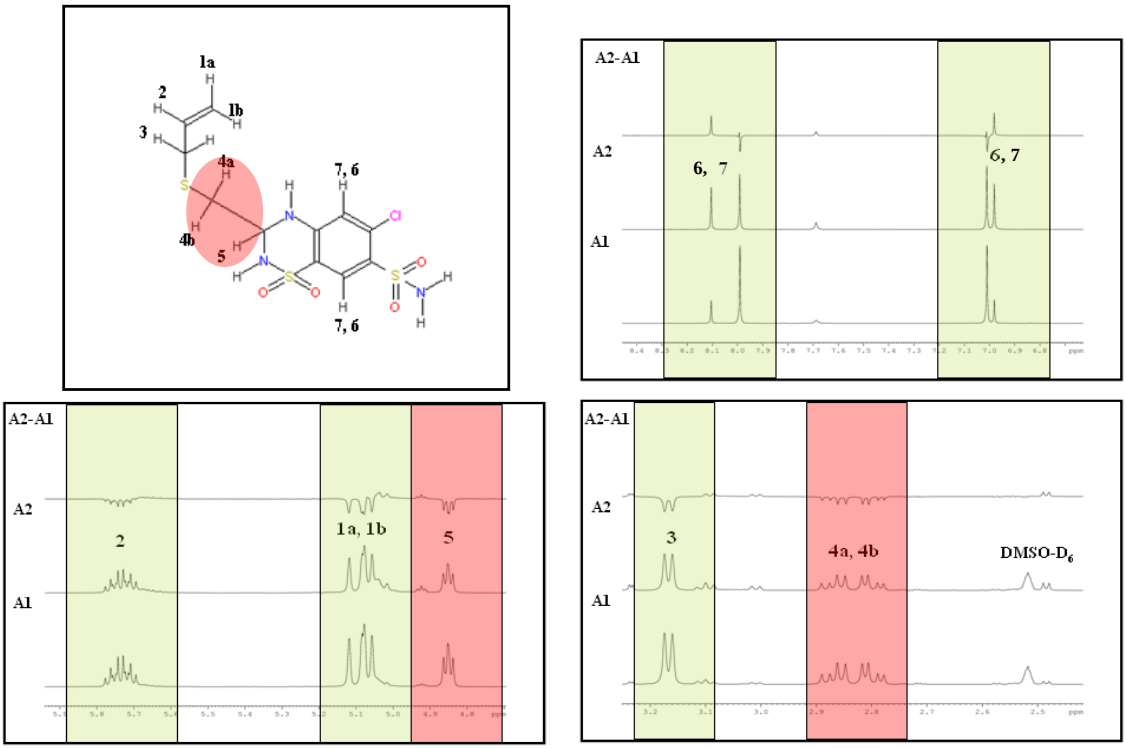

Figure 3-8. Magnified view of 1D 1H NMR spectra for Samples A1 and A2. Aromatic, aliphatic, and vinyl protons are highlighted in green. The significant ABX pattern is highlighted in red. The top leftmost panel is a key of the labeled hydrogens on althiazide.

CHAPTER 4
LIQUID CHROMATOGRAPHY-MASS SPECTROMETRY ANALYSIS OF ALTHIAZIDE

Introduction

Liquid chromatography is a physical method that separates a compound of interest from a complex mixture for the purposes of isolating, identifying, and quantitatively determining such a compound. Separation is dependent on the selective allocation of analytes between a liquid mobile phase and a stationary phase. In general terms, the sample is injected into the mobile phase stream where it is carried by a high-pressure pump and shipped through the column where the separation occurs (Tiller *et al.*, 2003). A flow-through detector monitors the separation. Qualitatively speaking, the primary shortcoming of liquid chromatography is its limited ability to provide unambiguous identification of the compounds of a mixture (Tiller *et al.*, 2003). Comparing the retention time of an unknown component with reference materials as determined under invariable experimental conditions is a means of identifying an unknown compound. However, because of the numerous amount of compounds present in the environment, it is not possible to say with absolute certainty that two compounds are the same. Additionally, the complete separation of components of a mixture may not always be feasible and thus may lead to the inaccurate identification of compounds.

Mass spectrometry exhibits high specificity for compounds and yields a high degree of confidence for determining unknown components. However, the mass spectrum obtained will contain ions from all compounds present in a mixture and consequently, if the compound of interest is a minor part of the mixture then identification of the analyte will be very difficult. Thus, combining liquid chromatography and mass spectrometry becomes beneficial because many compounds have similar retention characteristics but different mass spectra and can thus be distinguished from one another in a mixture.

LC-MS was used to verify the althiazide degradation product that was initially observed in the CA II and CA IX mimic crystal structure and to validate the results from the NMR studies.

Materials and Methods

Four solutions of varying concentrations of althiazide, (designated A, B, C, and D) were prepared. Samples A and B contained 50 mM Althiazide in 50 mM Tris-HCl. Each sample was solubilized in 30% DMSO. Samples C and D were composed of ~0.003 M althiazide in 50 mM Tris-HCl. Sample A was not exposed to heat and thus served as a control. Sample D was incubated with wt CA II (14.59 mg mL^{-1}) for 24 hours and was prepared as described in Chapter 3. After Samples B and C were left standing for ~24 hours, they were both submerged in a 70 °C water bath for 1 hour.

The samples were kept frozen in a -4 °C freezer until ~60-80 minutes prior to their analysis when they were removed and allowed to come to room temperature. They were subsequently analyzed via reverse phase gradient C18 HPLC/UV (275 nm)/(+)ESI-MSn. Mass spectrometry was performed with the ThermoFinnigan (San Jose, CA) LCQ system equipped with an electrospray ionization (ESI) (+)ESI: sheath gas (N2) = 65; aux gas(N2) =3; spray voltage = 3.3 kV; cap temperature = 250°C; cap voltage = 15 V; tube lens offset = 0 V. The (+)ESI scan event details were as follows:

1: Pos o(125.0-450.0) SID=1.0V.
2: Pos Dep MS/MS Most intense ion from (1). SID=1.0V.
3: Pos o(420.0-1000.0) SID=2.0V.
4: Pos Dep MS/MS Most intense ion from (3). SID=2.0V.
5: Pos Dep MSn Most intense ion from (4). SID=2.0V.
6: Pos o(950.0-2000.0) SID=3.0V.
7: Pos Dep MS/MS Most intense ion from (6). SID=3.0V.
8: Pos Dep MSn Most intense ion from (7). SID=3.0V.

Mass Dependent scans: 3u, 37.5%CID, q0.25, 30 ms.

HPLC was performed with an Agilent (Palo Alto, CA) 1100 series binary pump. Samples were loaded onto a Waters Atlantis dC18 column (2.1 x 150 mm, 3 μm particle) with a flow rate of 0.15 mL/min. They were injected with a Rheodyne 7125 manual injector with a 25 μL injection loop and a 25 μL Hamilton 1702 gastight syringe. The mobile phases were as follows: A= 0.2% HCOOH + ~1.2 μM NH_4 acetate + ~0.26 μM sodium acetate in H_2O (Burdick and Jackson); B = methanol (Burdick and Jackson). The gradient can be described by:A:B(min) = 100:0 (0) → 5:95 (45-65) → 100:0 (75-90). Samples were detected with an Agilent 1100 G1314A UV/Vis detector at a wavelength = 275 nm. MS spectra were collected in the 280 to 1300 *m/z* range.

Results

The HPLC/UV spectra had indicated that there were two large UV absorbing compounds present in all the samples with retention times of ~17 min and ~34 min (Figure 4-1). The RT 17 min large UV absorbing peak corresponded to the degraded compound while the RT 34 min peak correlated to althiazide. The (+) ESI mass spectra had shown that the RT 17 min compound had an *m/z* value of 286/288 and 308/310 (Figure 4-2). These ion clusters correspond to the $[M+H]^+$ and $[M+Na]^+$ ions of a 285 molecular weight compound. The degraded compound in sample A (50 mM althiazide + storage buffer alone) had comprised 39.5% of the total althiazide product; Sample B (50 mM althiazide + storage buffer + heat) had 53.2% of the degraded product; Sample C (~0.003 M althiazide + storage buffer + heat) had 64.9% of the degraded compound; Sample D had 70.7% of the degraded compound. Table 4-1 depicts the amount of degraded compound and the quantity of althiazide product present in all four samples.

Conclusions

The degraded compound had a molecular weight of 285 which aligns with the possibility that the tail of althiazide had in fact been cleaved (Figure 4-3). Since the 285 molecular weight

compound was present in all four samples, this suggests that the degradation of althiazide is a consequence of its environment. It appears that the more aggravated samples exhibited higher quantities of degraded compound. Subjecting the samples to various treatments such as heat, buffer, and enzyme all appeared to contribute to althiazide's instability. However, the primary cause of althiazide's scissioned tail cannot be attributed to any one source. Hence, further investigations need to be performed.

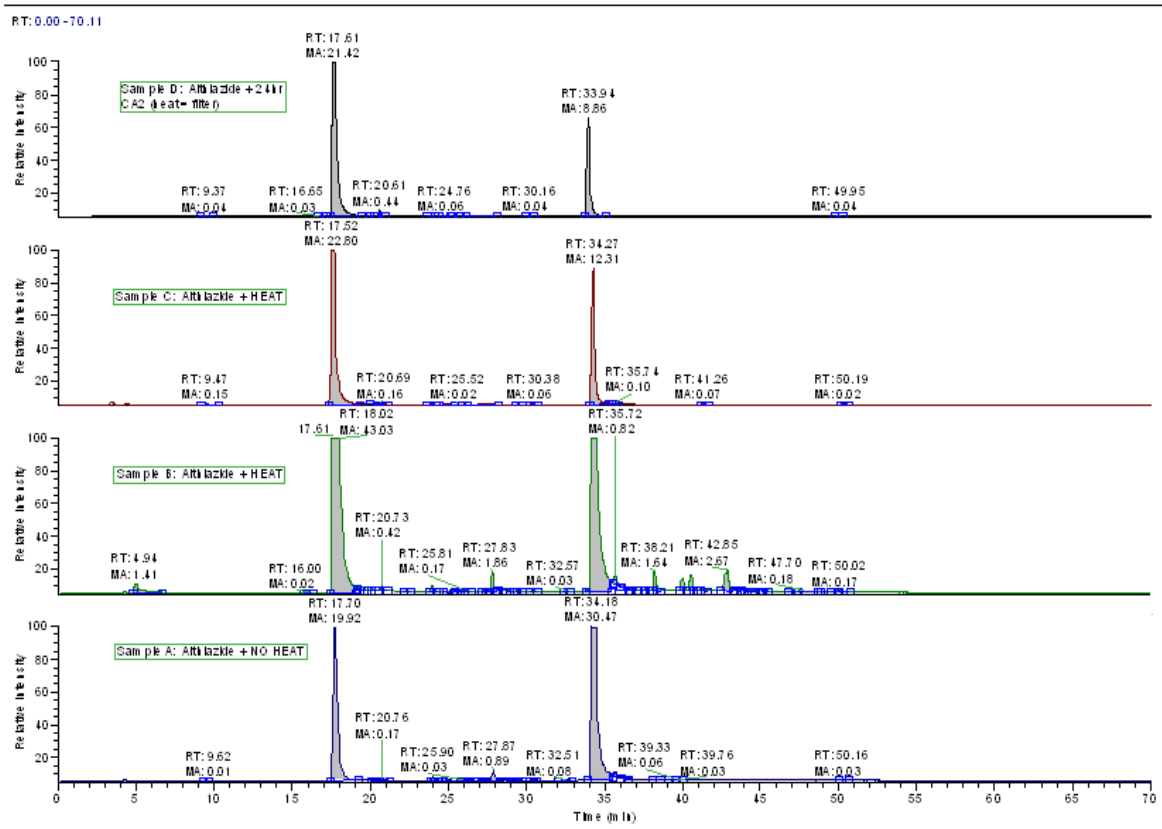

Figure 4-1. HPLC/UV (275 nm) spectra of samples A, B, C, and D. RT=retention time; MA:# is the manually integrated peak area (shaded).

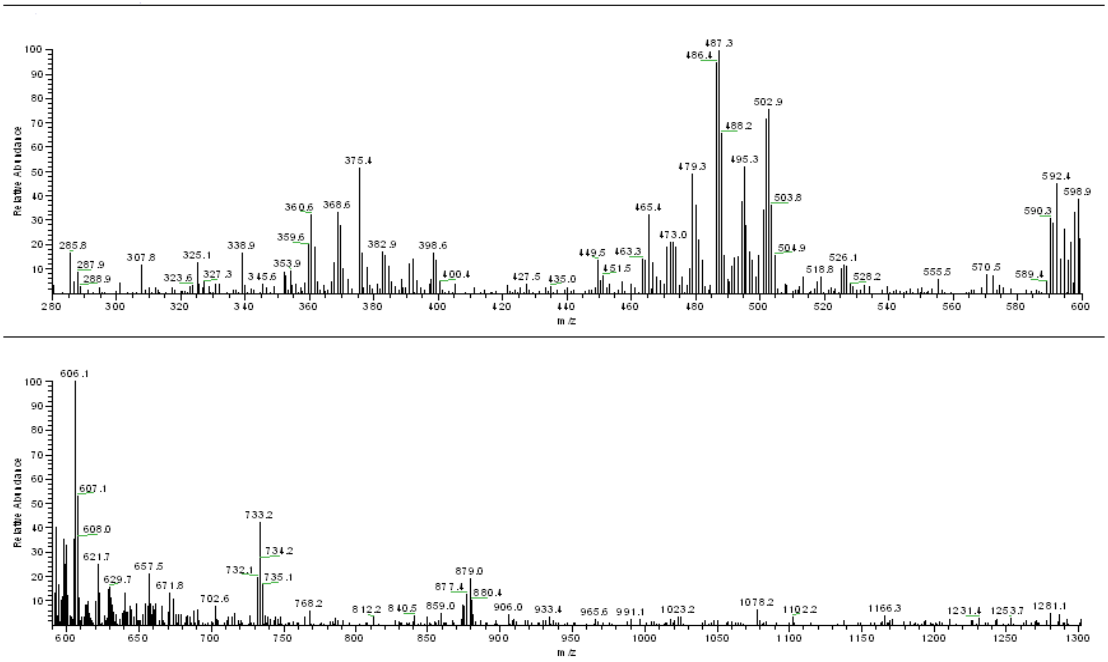

Figure 4-2. (+)ESI mass spectra of the RT 17.8 min large UV absorbing compound.

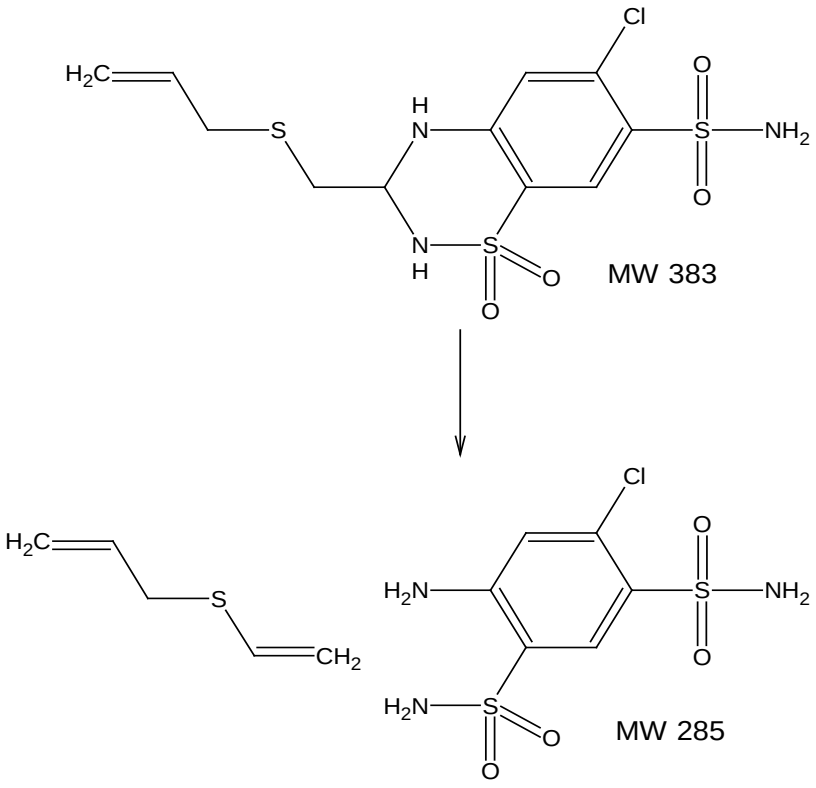

Figure 4-3. Schematic representation of possible degradation of althiazide.

Table 4-1. Quantitative comparison of integrated peak areas for RT 17 and RT 34.

Sample	Area			%Total Area	
	RT 17	RT 34	Total	RT 17	RT 34
Sample D	21.4	8.9	30.3	70.7	29.3
Sample C	22.8	12.3	35.1	64.9	35.1
Sample B	43.0	37.8	80.8	53.2	46.8
Sample A	19.9	30.5	50.4	39.5	60.5

CHAPTER 5
CRYSTALLIZATION AND STRUCTURAL ANALYSIS OF HUMAN CARBONIC ANHYDRASE II COMPLEXED WITH BISULFITE

Introduction

Temperature-dependent vibration of atoms in a crystal structure generates dynamic disorder in a crystal. This activity is defined by the temperature factor. Protein crystals also exhibit *static disorder* which are molecules are parts of molecules in different unit cells that do not continually reside in the exact position and do not have the exact same orientation (Drenth, 1994). Static disorder and dynamic disorder have the same effect on X-ray diffraction and thus cannot be differentiated unless the intensity data at various temperatures are obtained. Since there is disorder in the crystal, the diffraction pattern fades away at some diffraction angle θ_{max}. The lattice distance d_{min} can then be determined by Bragg's law (Equation 5-1) (Drenth, 1994):

$$d_{min} = \lambda/2\sin\theta_{max} \quad (5\text{-}1)$$

d_{min} is the resolution of the diffraction pattern. The accuracy of a crystal structure is strongly dependent on the diffraction pattern's resolution. In addition, a data set completeness of 80% or better is generally sufficient for good quality data.

Presently, our knowledge on the binding of the metal-complexing anions to the Zn(II) ion of carbonic anhydrase is based on crystal structures with lower resolutions and significantly lower data set completeness (Table 5-1). Hence, this begs the need to reinvestigate the manner in which these anions bind to the enzyme's active site. This chapter deals with the specific binding patterns of the bisulfite anion.

Methods

Expression and Purification

Wild type hCA II was expressed in E. coli BL21(DE3)pLYSs and purified by affinity chromatography as described in Chapter 2.

Crystallization

Crystals of wt hCAII were prepared by the hanging drop diffusion method (McPherson, 1982). The reservoir solutions contained a mixture of ammonium sulfate (2.4 M) and 100 mM of Tris-HCl at a pH of 8.0. Each drop had a 5:5 ratio of protein (at ~25 mg mL^{-1} in 50 mM Tris-HCl, pH 7.8) to precipitant solution for a total volume of 10 μL. The drops were pendent over 1 mL precipitant solution. Within 7 days, crystals were observed.

Sodium bisulfite was solubilized in water. 2 μL of sodium bisulfite (0.3 M pH 7.3) was added to the CA II crystal at room temperature for ~24 hours prior to data collection.

Diffraction Data Collection

X-ray diffraction data sets were collected on an in-house R-AXIS VII++ image plate system with a Rigaku generator as described in Chapter 1. There was a total of 26, 978 reflections measured to a maximum resolution of 1.7 Å. The crystal belongs to the $P2_1$ space group with unit cell parameter of a=42.8 Å, b=41.6 Å, c=72.6 Å, and β=104.4 °. The data set had 2630 (97.7% complete) independent reflections. The data was indexed using *DENZO* and scaled with *SCALEPACK* using HKL2000 (Otwinowski, 1997). The structure had an R_{symm}=0.068. The data collection statistics are given in Table 5-2.

Phasing, Model Building, Refinement Protocol

The CA II crystal structure complexed with bisulfite was phased with the molecular replacement method using the software packages, Crystallography and NMR System (CNS) (Brunger, 1998). The phasing model used was obtained from the Protein Data Base, accession number 2ILI (Fisher *et al.*, 2007), from which all the water molecules were removed. The standard refinement protocol of CNS was used to refine the structure. Fo-Fc Fourier electron-density maps were generated after one cycle of rigid-body refinement, annealing with gradual cooling, geometry restrained position refinement and temperature-factor refinement (Brunger,

1998). Difference Fourier maps yielded distinct, phase-unbiased electron density for the bound inhibitors. During the refinement process, the PRODRG server was used to generate the topology files for modeling the sulfite structure (Schuttelkopf & van Aalten, 2004). The computer graphics program COOT (Emsley & Cowtan, 2004) was used to manually model the structure. Refinement of the structures continued until convergence of R_{cryst} and R_{free} was attained. The ligand and protein interactions were accessed by observing the environmental distances in COOT. *PROCHECK* (Emsley & Cowtan, 2004, Laskowski *et al.*, 1993). Table 5-2 and 5-3 show the data-refinement and final model statistics.

Results

Figure 5-1 shows the binding of the sulfite ligand in the active site of the enzyme. The data was isomorphous with the other HCA II crystal structures. Overall, the refined model had good geometry with root-mean-square deviations for bond lengths and angles of 0.012 and 1.60 respectively. The main chain and the side chain atoms had average *B* values of 17.2 and 24.0, respectively. The bisulfite ligand had an average *B* factor of 19.1. There were 263 water molecules added to the model with an average *B* value of 34.6 (Table 5-3). The final refined model had an R_{cryst} of 18.7% and an R_{free} of 19.3%.

Hakansson *et al*. claims that bisulfite has a puckered conformation instead of a planar geometry (Hakansson, 1992). However, data from the newly solved wt CAII-bisulfite structure depicts otherwise; in the wt CAII-bisulfite crystal structure presented here, bisulfite appears planar (Figure 5-2). The OAD atom replaces the zinc water in the native structure. The distance between OAD and the zinc ion is 2 Å. The difference in position between the OAD atom and the zinc-bound water in the native structure is only 0.1 Å. The Zn(II) ion is still tetrahedrally coordinated. OAD and T199Oγ1 are separated by a distance of 2.5 Å. The OAC atom is 2.5 Å

from the T199 N and 3.8 Å from T199Oγ1. Water 128 is within hydrogen bond distance to the sulfite. It is 2.7 Å from OAA and 3.5 Å from OAC. This water is not observed in the native structure. The same residues from the Hakansson data, Thr199, Leu198, Val121, Val143, and Trp209, still surround the bisulfite anion. Important ligand-amino acid residue interactions are displayed in Table 5-4.

A comparison of the previously solved CAII-bisulfite complex structure and the current CAII-bisulfite structure shows markedly distinct differences in the geometric conformation of the bisulfite ligand. The O3 atom, which corresponds to the OAC atom from the current data, is separated from the Zn(II) by 2.1 Å. It has a difference in position of 0.1 Å. O3 is 2.8 Å away from T199Oγ1 with a difference in position of 0.3 Å from the current data. The O1 atom (corresponding to the OAC atom), is 2.9 Å away from T199 N and is 3.9 Å away from T199Oγ1, with a difference in position from the current data of 0.3 Å and 0.1 Å respectively. Water 389 (corresponding to 128) is 2.7 Å away from O2 and 3.0 Å away from O1, with a difference in position of 0.1 Å and 0.5 Å respectively (Table 5-4).

Conclusion

After reassessing the manner by which bisulfite binds to the Zn(II) ion of the CAII active site, it is evident that there are some noticeable differences from the crystal structure presented here and the CAII-bisulfite crystal structure solved by Hakansson *et al*. While the Zn(II) ion is tetrahedrally coordinated, there are still some variations in the geometric conformation of the bisulfite ligand. OAD and O3 both replace the zinc-bound water molecule that was present in the native structure. OAD is 2.0 Å away from the Zn(II) ion and differs in location from the original structure by 0.1 Å. A hydrogen bonding network is observed around the bisulfite ligand. OAD acts as a proton acceptor and hydrogen bonds with T199Oγ1 and is separated by a distance

of 2.5 Å while the OAC atom is 2.5 Å away from T199N as well. Additionally, OAA is 2.7 Å away from water 128. Since the electron density of bisulfite indicates that it has a planar geometry, this suggests that one of the oxygens on the ligand is protonated and thus acts as a proton donor. A puckered geometric conformation would suggest that the sulfur is protonated which does not appear to be the case in the structure presented here. The structure solved by Hakannson *et al*. has a less cohesive hydrogen bonding network. O3 is separated from T199Oγ1 by 2.8 Å; O1 is 2.9 Å away from T199 N while O1 and O2 are separated from the corresponding water 128 by distances of 3.0 Å and 2.7 Å respectively. This looser hydrogen bonding network that is observed in the original CAII-bisulfite structure suggests that the S atom is protonated as opposed to the O atoms which gives rise to its trigonal pyramidal geometry.

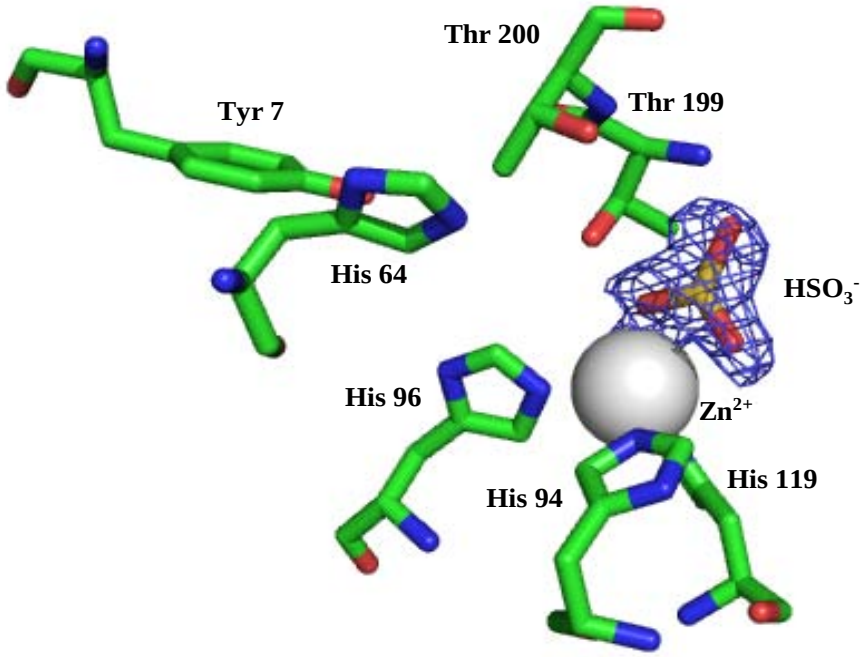

Figure 5-1. Crystal structure of wt human CA II complexed with bisulfite. The 2Fo-Fc electron density map is contoured at 1.5 σ. Zn^{2+} atom is shown as a gray sphere. HSO_3^- is shown interacting with the active site residues. Atom coloring is as follows: carbon (green), oxygen (red), nitrogen (blue), sulfur (orange). Figure was generated in PyMol (DeLano, 2002).

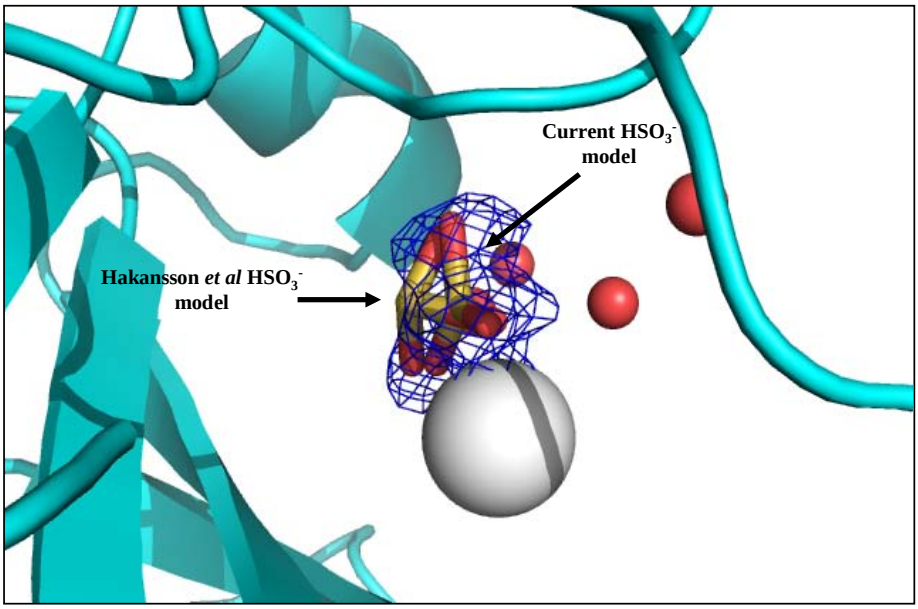

Figure 5-2. Crystal structure of CA II complexed with bisulfite. Ligand obtained from Hakansson model is superimposed on current crystal structure presented here. Zn^{2+} atom is shown as a light gray sphere. Water molecules are colored red. Ribbons and arrows convey helices and β-strands, respectively. The 2Fo-Fc electron density map is contoured at 1.5 σ. Figure was generated in PyMol (DeLano, 2002).

Table 5-1. Data comparison of previously solved crystal structures of CA II complexed with anions

Anion	PDB Accession Number	Previous Data Resolution and Completeness
[a]Sulfite	2cbd	1.67 Å, 65.8%
[a]Formic Acid	2cbc	1.88 Å, 61.2%
[a]Cyanamide	1f2w	1.9 Å, 89.8%
[b]Azide	1ray	1.8 Å, 65.6%
[b]Bromide	1raz	1.9 Å, 54.5%

[a]Hakansson, K., Carlsson, M., Svensson, L.A., Liljas, A. (1992). *J Mol Biol* **4**, 1192-1204.
[b]Jonsson, B. M., Hakansson, K. & Liljas, A. (1993). *FEBS Lett* **322**, 186-190.

Table 5-2. . X-ray crystallographic data collection statistics for wt human CA II complexed with bisulfite.

Data Set Statistics	wt CAII-bisulfite
Space Group	$P2_1$
Unit-cell parameters (Å,°)	*a*=42.8 *b*=41.6 *c*=72.6 β=104.4
Resolution (Å)	50-1.7 (1.76-1.7)
Total number unique reflections	26978 (2630)
Redundancy	1.9
Completeness (%)	97.7 (96.4)
R_{symm}	0.068

[a] $R_{symm} = \Sigma |I - \langle I \rangle| / \Sigma \langle I \rangle$.

Table 5-3. X-ray crystallographic refinement statistics for wt human CA II complexed with bisulfite

Model Statistics	
R_{cryst} [a]	0.182
R_{free} [b]	0.193
Rmsd for bond lengths (Å)	0.012
Rmsd for angles (°)	1.6
Average B-Factors (Å^2)	
Main/side/solvent/drug	17.2/24.0/34.6/19.1
Ramachandran Statistics (%)	
Preferred/Allowed/ Outliers	93.6/6.0/0.4
No. protein atoms	261
No. water molecules	263

[a] $R_{cryst} = \Sigma |F_o| - |F_c|/\Sigma |F_{obs}| \times 100$. [b] R_{free} is calculated in the same fashion as R_{cryst}, except that it uses 5% of the reflection data omitted from refinement.

Table 5-4. Protein-Ligand Interactions

Bisulfite (97.7% Data Set Completeness)	wt hCA II residue	Distance (Å)
OAD	Zn	2.0
OAD	Oγ1Thr199	2.5
OAC	NThr199	2.5
OAC	Oγ1Thr199	3.8
OAA	W128	2.7
OAC	W128	3.5
Bisulfite (65.8% Data Set Completeness)	wt hCA II residue	Distance (Å)
O3	Zn	2.1
O3	Oγ1Thr199	2.8
O1	NThr199	2.9
O1	Oγ1Thr199	3.9
O2	W389	2.7
O1	W389	3.3

CHAPTER 6
KINETIC STUDIES OF INHIBITION OF CARBONIC ANHYDRASE II

Oxygen-18 Isotope Exchange Kinetic and Inhibition Studies

Introduction

The ^{18}O exchange activity between CO_2 and water can be used to assess the inhibition (K_i) constants of the drug compounds. This method is an equilibrium method that is used to determine the role of proton transfer in the pathway of the catalytic hydration for CO_2. Additionally, when bicarbonate ^{18}O-labeled, this method shows the rate of release of oxygen from the enzyme (Silverman, 1982). ^{18}O exchange is a result of the hydration-dehydration cycle that occurs at chemical equilibrium (Silverman, 1982). It exchange occurs in two steps. First, ^{18}O-labeled bicarbonate is dehydrated, yielding CO_2. During the second step, which occurs independently of step 1, labeled oxygen is released to solvent water (Equation 6-1) (Silverman, 1982).

$$CO^{18}O + H_2O \underset{k'_{31}}{\Leftrightarrow} HCOO^{18}O^- + H+ \underset{k'_{13}}{\Leftrightarrow} COO + H_2{}^{18}O \qquad (6\text{-}1)$$

The rate of oxygen exchange between water and carbon dioxide can be determined by the pH of the solution. The rate constant k'_{31} measures the hydration of CO_2 in acidic solution. Using the ^{18}O exchange method provides several advantages to measuring the kinetics of catalyzed CO_2 hydration. Since ^{18}O exchange is an equilibrium method, there is no change in pH and thus, the buffer concentration becomes inconsequential to the reaction (Silverman, 1982). Small quantities of ^{18}O can be used because of the mass spectrometer's high sensitivity to CO_2. Because the rate of ^{18}O exchange is a slow kinetic method used to determine the rates of catalysis by one of the fastest enzymes, this method calls for as low as nanomolar concentrations of carbonic anhydrase (Silverman, 1982). Thus, ^{18}O exchange has proven to be very beneficial

in detecting small amounts of enzyme. Several studies of native and metal-substituted carbonic anhydrases have indicated that the pH and the enzyme's catalytic activity and its inhibition are all interrelated components of CA involving the metal ion. Additional factors such as the various differences in isozymes, the solution's ionic strength, and the presence of inhibitors also appear to affect the apparent pK_a of carbonic anhydrase(Silverman, 1982).

Methods

The inhibition constant (K_i values) for CA II with acetazolamide, benzthiazide, chlorthalidone, and hydroflumethiazide was determined by measuring the inhibition of ^{18}O-exchange activity between CO_2 and water through the use of mass spectrometry. Additionally, because HPLC/MS studies had showed that Sample A was predominantly comprised of non-degraded althiazide (60.5%) and Sample D was predominantly composed of degraded althiazide (70.7%), the inhibition constants for CA II with the HPLC samples were determined in order to compare the relative inhibitory effects of the non-degraded althiazide versus the degraded althiazide on CA (refer to Chapter 4 for sample preparation). The experiments were conducted at 10°C in 0.1 M Hepes buffer at pH 7.4. The total bicarbonate concentration was 10 mM; wt CA II concentration was at 9.75 μM and inhibitor concentrations varied from 1 μM to 5 mM. K_i values were subsequently determined by the Henderson method for tight-binding inhibitors (Segel, 1975).

Results

The inhibition constant for acetazolamide, a widely established CA inhibitor, was reassessed to compare the relative rates of inhibition of CA II by althiazide, benzthiazide, chlorthalidone, and hydroflumethiazide. Acetazolamide showed the highest inhibition potency over the various inhibitors that were tested. Out of the inhibitors that were analyzed,

benzthiazide exhibited the strongest inhibitory effects against CA II with a K_i of 0.0682 ± 0.0103 μM (Figure 6-1). Chlorthalidone and hydroflumethiazide showed moderate inhibitory effects with K_i values of 0.102 ± 0.0034 μM and 0.942 ± 0.26 μM respectively (Figures 6-2 and 6-3). Sample D (70.7% degraded althiazide) exhibited an 18-fold higher potency over Sample A (60.5% non-degraded althiazide) with K_i values of 1.97 ± 0.427 μM and 45 ± 1.19 μM for samples D and A respectively (Figures 6-5 and 6-4). Table 6-1 displays the K_i values for the inhibitors.

Conclusion

The sulfonamide group is a key feature of the majority of the inhibitors analyzed which further reaffirms the observation that sulfonamides act as CA inhibitors. Acetazolamide, an established CA inhibitor, exhibited the greatest binding affinity for CA II followed by benzthiazide, chlorthalidone, and hydroflumethiazide. In addition, the degraded althiazide acted as a more potent inhibitor than the non-degraded althiazide.

After equilibrium with the enzyme, acetazolamide behaves as a reversible noncompetitive inhibitor in the absence or presence of substrate (Leibman *et al*., 1960). Benzthiazide has the inherent property of significantly increasing in inhibitory potency with time as it comes into equilibrium with CA in the absence of substrate (Leibman *et al*., 1960). Leibman *et al* reports that carbon dioxide protects CA from inhibition by benzthiazide.

Benzthiazide, chlorthalidone, and althiazide incorporate a 2-chlorobenzenesulfonamide moiety. While these compounds possess similar chemical structures and shapes, their CA inhibition profiles are different. Of the inhibitors tested, hydroflumethiazide is the only group of sulfonamides that lack the 2-chlorobenzenesulfonamide moiety and does not significantly inhibit CA II.

The bulky tail that is present in the non-degraded althiazide may prevent it from binding to the enzyme's active site. Consequently, this may account for Sample A's weaker binding affinity to CA II. Because the tail is scissioned in the degraded althiazide, sample D, the inhibitor encounters less steric hindrance with the active site residues and thus has a tighter binding affinity for CA II.

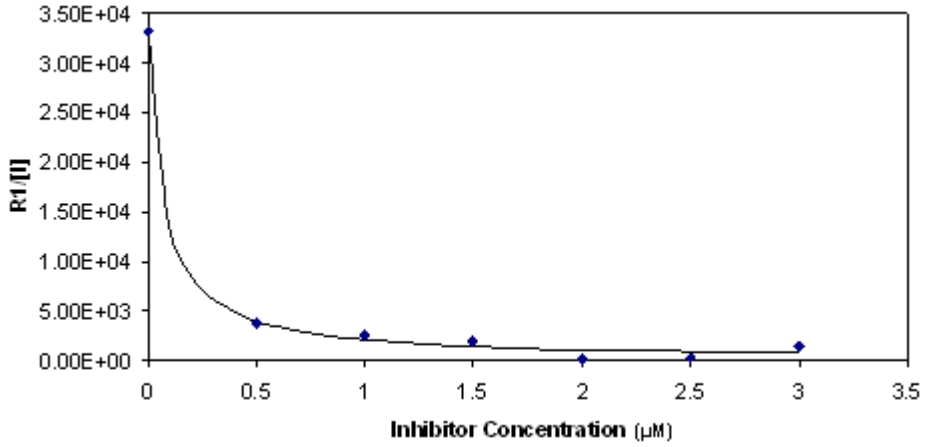

Figure 6-1. Rate of hydration/dehydration for wt human CA II over increasing benzthiazide concentration range. R1 is the hydration/dehydration rate and E is the enzyme concentration.

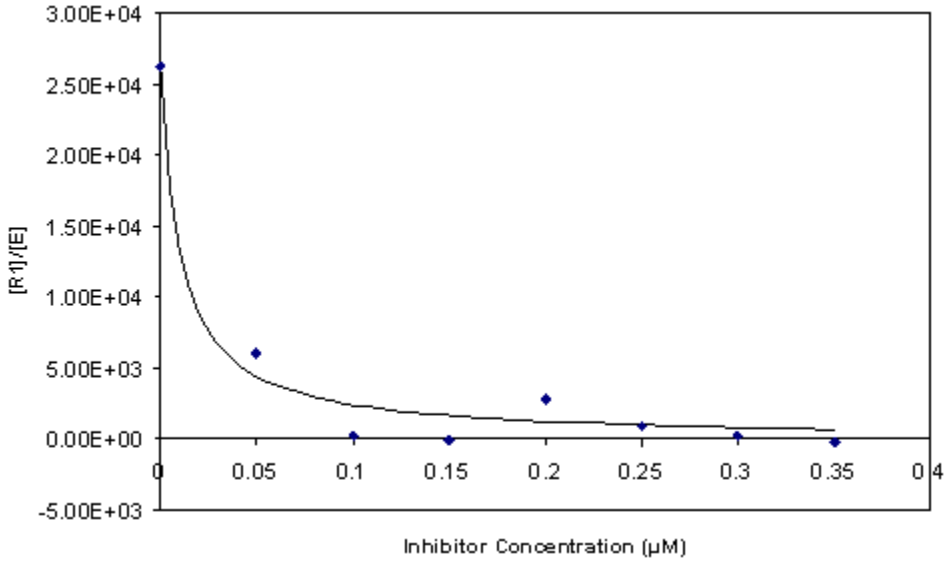

Figure 6-2. Rate of hydration/dehydration for wt human CA II over increasing chlorthalidone concentration range. R1 is the hydration/dehydration rate and E is the enzyme concentration.

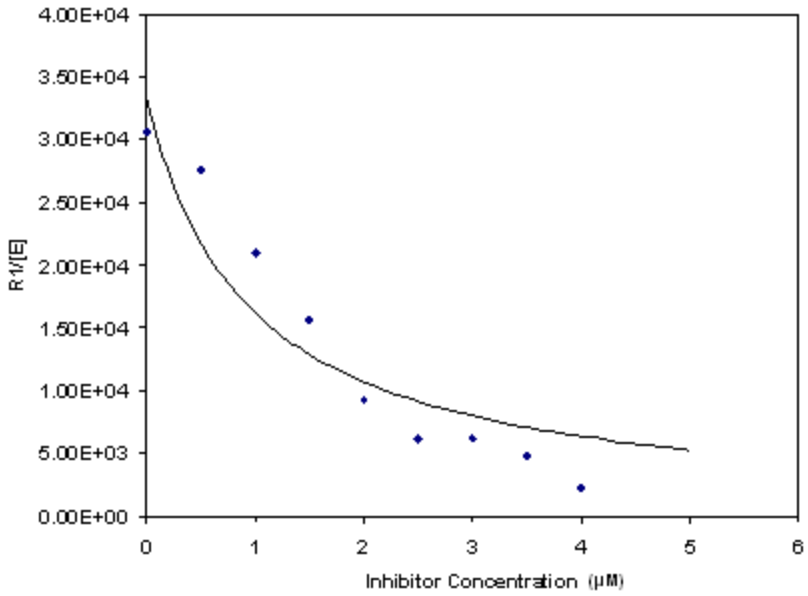

Figure 6-3. Rate of hydration/dehydration for wt human CA II over increasing hydroflumethiazide concentration range. R1 is the hydration/dehydration rate and E is the enzyme concentration.

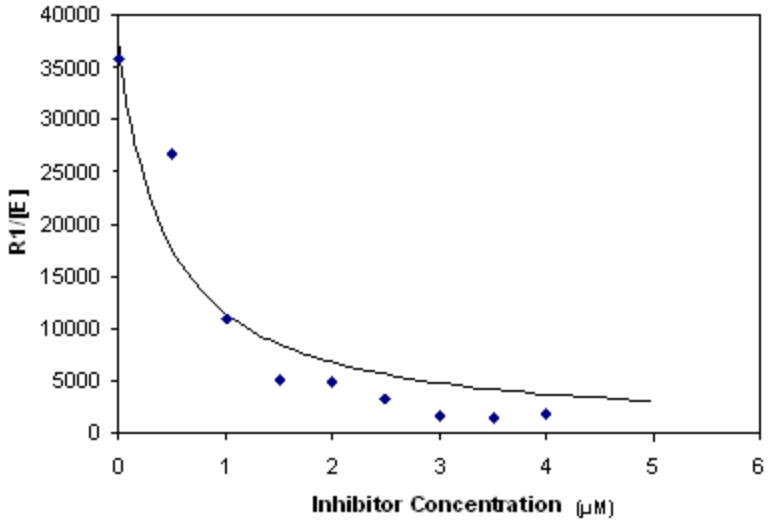

Figure 6-4. Rate of hydration/dehydration for wt human CA II over increasing althiazide (Sample A: 60.5% non-degraded althiazide) concentration range. R1 is the hydration/dehydration rate and E is the enzyme concentration.

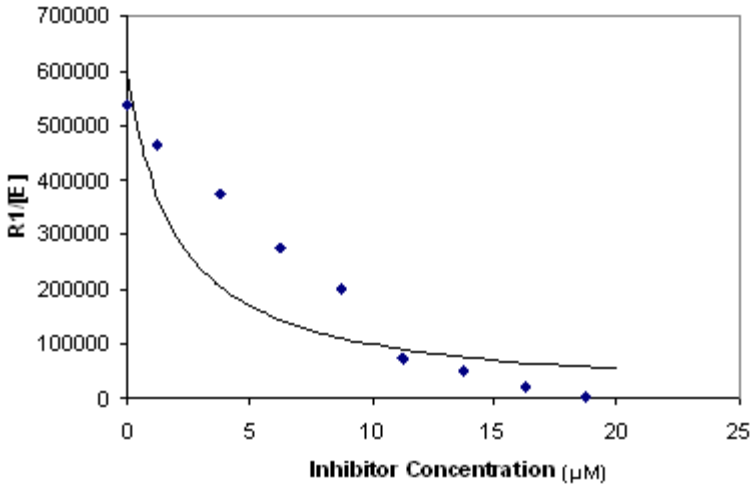

Figure 6-5. Rate of hydration/dehydration for wt human CA II over increasing althiazide (Sample D: 70.7% degraded althiazide) concentration range. R1 is the hydration/dehydration rate and E is the enzyme concentration.

Table 6-1. Ki values (μM) of Inhibitors for CA II

Inhibitor	CA II
Acetazolamide	0.00693 ± 0.0076
Benzthiazide	0.0682 ± 0.0103
Chlorthalidone	0.102 ± 0.0034
Hydroflumethiazide	0.942 ± 0.26
Sample A: 60.5% Non-Degraded Althiazide	45 ± 1.19
Sample D: 70.7% Degraded Althiazide	1.97 ± 0.427

CHAPTER 7
CONCLUSIONS

The principle goal of this investigation was to enhance the understanding of carbonic anhydrase inhibitors and their binding mechanism. The fact that CA II and CA IX may serve as useful targets in treating various diseases begs the need for the search of highly potent inhibitors. While sulfonamides have already been clinically established as effective CA inhibitors, the problem of isolating isozyme-specific inhibitors still exists. The results reported in the preceding chapters have fully achieved this objective. The experimental techniques that were employed throughout these studies have not only yielded valuable information regarding the specific binding patterns of CA inhibitors, but have also proven that common drugs that are used for medical treatment may in fact be unstable.

Althiazide is a benzothiadiazine derivative that belongs to a class of diuretics used for treating hypertension and has been shown to possess some inhibitory effects on renal carbonic anhydrases. The 1.5 Å and 1.6 Å resolution crystal structure of althiazide in adducts with CA II and CA IX mimic has provided the fundamental framework for determining the drug's binding pattern and chemical nature as well. Upon completion of this investigation, X-ray crystallography has proven that althiazide binds to the active site of two carbonic anhydrase isozymes, CA II and CA IX mimic. Althiazide typifies the binding profile of sulfonamides, with the nitrogen atom directly coordinated to the Zn(II) ion and the heterocyclic region interacting with the hydrophobic amino acid residues of the active site. Interestingly, a lack of electron density surrounding the compound's tail region has provided the initial evidence that althiazide may be a mutable inhibitor and may also be unstable. This prompted the need for further investigation on the compound's aberrant behavior.

NMR spectroscopy was employed in order to determine whether or not the degradation of althiazide was a function of two parallel pH-dependent pathways or was a result of the internal interactions occurring between althiazide and the active site residues of carbonic anhydrase. Experiments that assessed althiazide's response to various environmental conditions have suggested that it is a relatively resilient compound. 1D ^{1}H NMR spectroscopy in particular has identified an ABX pattern among alkaline, neutral, and acidic solutions of althiazide, suggesting that althiazide's tail region remained intact when extreme adjustments in pH were applied to the drug. Delving further into the matter, althiazide was reanalyzed to determine if the carbonic anhydrase active site environment had scissioned the compound's tail. Four solutions (designated A, B, C, and D) were prepared. All solutions were solubilized in ~50% DMSO-D6. Samples A and D were designed in order to assess althiazide's structural stability in CA storage buffer alone. In sample A, althiazide was incubated in CA storage buffer (50 mM Tris-HCl pH 7.8) and in sample D, the drug was left in PBS (pH 7). In samples B and C, althiazide was exposed to varying concentrations of wt human CA II. All four samples were left standing in solution for ~ 24 hours prior to heat treatment. Samples B and C were subjected to heat treatment in order to denature the protein and release the inhibitor from the active site. Samples A and D were subsequently heated to confirm that the heat treatment in samples B and C did not contribute to the degradation of althiazide. The results had indicated that the distinctive ABX pattern was still manifest in solutions which were not exposed to carbonic anhydrase, notably samples A and D. However, samples which were exposed to carbonic anhydrase, (B and C), did not exhibit the ABX pattern, thus suggesting that the degraded compound may be a result of the chemical interactions that are occurring within the active site of the enzyme.

Additional analysis on the nature of althiazide was investigated this time through the use of HPLC/MS. Four samples (designated A, B, C, and D) were assessed to determine the mass of the possible degraded compound. Samples A and B were both comprised of 50 mM Althiazide in 30% DMSO and CA storage buffer (50 mM Tris-HCl). Samples C and D both contained ~0.003 M althiazide in CA storage buffer. Only sample D was exposed to wt human CA II. Samples B, C, and D were all subjected to heat treatment. Samples were analyzed via reverse phase gradient C18 HPLC/UV (275 nm)/(+) ESI-MSn. The results had indicated that there were two large UV-absorbing compounds in each of the four samples with retention times of ~17 and ~34 min respectively, The RT 17 min large UV absorbing compound related to the degraded compound, while the RT 34 min compound corresponded to althiazide). The (+)ESI mass spectra of the RT 17 min compound had an *m/z* value of 286/288 and 308/310 which may relate to the $[M+H]^+$ and $[M+Na]^+$ ions of a 285 molecular weight compound. The amount of the degraded compound in the althiazide product in all four samples can be observed in Table 4-1. The results indicate that the degraded compound was present in varying degrees in all four samples. Sample A, the sample which was not subjected to heat nor exposure to enzyme, had the least amount of degraded compound present; of which the degraded compound had comprised ~40% of the amount of althiazide. Sample D (heat + enzyme treatment) had the highest quantity of degraded compound present of which the degraded compound had comprised ~71% of the total althiazide.

The exact causes of althiazide's deterioration, however, have not yet entirely been resolved from theses studies. As it stands, the compound does indeed appear to have a labile tail that is susceptible to cleavage from its heterocyclic ring. While NMR spectroscopy insinuates that carbonic anhydrase may be the sole factor contributing to althiazide's instability, additional

studies via HPLC/MS show that the compound's degradation may be a function of its environment. The addition of heat and enzyme to the sample appeared to exacerbate the degree of deterioration which was already manifested in the compound. The HPLC/UV spectra unequivocally show that there are two compounds present in all of the analyzed samples, each of which correlating to a molecular weight compound of 285 and althiazide. The crystal structures of both CA II and CA IX mimic complexed with althiazide, however, demonstrate that the degraded compound acts as a more effective inhibitor than althiazide since it was not obvious from the electron density maps that the entire althiazide structure was bound to the enzyme's active site. Kinetic studies further confirm that the degraded althiazide acts as a more potent inhibitor than the non-degraded althiazide. Steric hindrance with the active site residues may prevent the compound's tail from securely binding which may contribute to althiazide's degradation.

While the binding mechanism for metal-complexing anions have already been reported in the literature, our knowledge of these specific binding patterns are based on crystal structures with lower resolution and significantly lower data set completeness (Table 5-1). This prompted the need to reinvestigate the manner in which these small anions bind to the enzyme's active site. Hakansson *et al*. claims that bisulfite (data set completeness: 67.5%) has a puckered conformation. The 1.7 Å resolution structure (data set completeness: 97.7%) of CA II complexed with bisulfite presented in the preceding chapters show distinct differences in the ligand's structure. Contrary to the assertion made by Hakansson, bisulfite appears to have a planar conformation as opposed to a puckered geometry. Additional variations in the ligand's position within the active site are also observed in the current crystal structure. The differences

in geometry and position of bisulfite affirm the importance of a complete data set and show that the reassessment of the binding patterns of metal-complexing anions is necessary.

. ^{18}O exchange kinetics via mass spectrometry was employed in order to determine the inhibition constants of various compounds which included acetazolamide, althiazide, benzthiazide, chlorthalidone, and hydroflumethiazide. The results from this study confirmed that sulfonamides act as effective inhibitors. Of the compounds tested, benzthiazide, chlorthalidone, and althiazide share a 2-chlorobenzenesulfonamide moiety. Despite their similarities in chemical structure and shape, their inhibition profiles were different. Hydroflumethiazide lacks the 2-chlorobenzenesulfonamide moiety and acts as a weaker inhibitor. Additionally, the degraded althiazide acts as a significantly more effective inhibitor for CA than the non-degraded althiazide. The results from this study thus prove that there are additional intrinsic properties that are characteristic of certain compounds that seem to affect the nature of its inhibition.

The primary goal of this study was to identify the binding patterns of CA inhibitors and to assess its structural integrity within the active site of carbonic anhydrase. The results from the NMR and HPLC/MS studies could not be reconciled, and thus a more rigorous investigation on the nature of althiazide's chemical instability still needs to be performed. In addition, a more scrupulous examination of the metal-complexing anions need to be executed because of the disparities in position and geometric conformation that are observed in lower resolution and lower data set completeness crystal structures. Overall, the search for highly potent, isozyme-specific inhibitors for the various members of the CA family is a continuous study that relies on the bridging of information from all realms of biology and chemistry.

LIST OF REFERENCES

1. Abbate, F., Casini, A., Scozzafava, A. & Supuran, C. T. (2003). *J Enzyme Inhib Med Chem* **18**, 303-308.

2. Akitt, J. W. (1983). *NMR and Chemistry*. New York: Chapman and Hall.

3. Alberti, G., Bertini, I., Luchinat, C. & Scozzafava, A. (1981). *Biochim Biophys Acta* **668**, 16-26.

4. Baird, T. T., Jr., Waheed, A., Okuyama, T., Sly, W. S. & Fierke, C. A. (1997). *Biochemistry* **36**, 2669-2678.

5. Banci, L., Bertini, I., Luchinat, C., Monnanni, R., and Moratal Mascarell, J. (1989). *Gazzetta Chimica Italiana* **119**, 23-29.

6. Bertini, I., and Luchinat, C. (1983). *Accounts of Chemical Research* **16**, 272-279.

7. Bertini, I., Canti, G., Luchinat, C. & Borghi, E. (1983). *J Inorg Biochem* **18**, 221-229.

8. Bertini, I., Canti, G., Luchinat, C. & Scozzafava, A. (1977). *Biochem Biophys Res Commun* **78**, 158-160.

9. Bertini, I., Canti, G., Luchinat, C., and Mani, F (1981). *Journal of the American Chemical Society* **103**, 7784-7788.

10. Bertini, I., Canti, G., Luchinat, C., and Scozzafava, A. (1978). *Journal of the American Chemical Society* **100**, 4873-4877.

11. Bertini, I., Luchinat, C., Monnanni, R. & Scozzafava, A. (1982). *J Inorg Biochem* **16**, 155-160.

12. Bertini, I., Luchinat, C. & Scozzafava, A. (1977). *J Am Chem Soc* **99**, 581-584.

13. Briganti, F., Mangani, S., Scozzafava, A., Vernaglione, G. & Supuran, C. T. (1999). *J Biol Inorg Chem* **4**, 528-536.

14. Brunger, A. T., Adams, P.D., Clore, G.M., DeLano, W.L., Gros, P., Grosse-Kunstleve, R. W., Jiang, J.S., Kuszewski, J., Nilges, M., Pannu, N.S., Read, R.J., Rice, L. M., Simonson, T., and Warren, G. L. (1998). *Acta Crystallography Section D* **54**, 905-921.

15. Cavanagh, J., Fairbrother, W.J., Palmer, A. G., Skelton, N. J., Rance, M. (1996). *Protein NMR spectroscopy: principles and practice*. San Diego: Academic Press.

16. Coleman, J. E. (1975). *Annu Rev Pharmacol* **15**, 221-242.

17. Conway, J. & Lauwers, P. (1960). *Circulation* **21**, 21-27.

18. Corcoran, A. C., Macleod, C., Dustan, H. P. & Page, I. H. (1959). *Circulation* **19**, 355-359.

19. Danley, D. E. (2006). *Acta Crystallogr D Biol Crystallogr* **62**, 569-575.

20. Davenport, H. W., and Fisher, R.B. (1938). *Journal of Physiology* **94**, 16P-17P.

21. DeLano, W. L. (2002). *Delano Scientific*.

22. Dollery, C. T., Harington, M. & Kaufmann, G. (1959). *Lancet* **1**, 1215-1218.

23. Drenth (1994). *Principles of Protein X-ray Crystallography*. New York City, NY: Springer-Verlag New York, Inc.

24. Dustan, H. P., Cumming, G. R., Corcoran, A. C. & Page, I. H. (1959). *Circulation* **19**, 360-365.

25. Dustan, H. P., Page, I. H. & Poutasse, E. F. (1959). *N Engl J Med* **261**, 647-653.

26. Emsley, P. & Cowtan, K. (2004). *Acta Crystallogr D Biol Crystallogr* **60**, 2126-2132.

27. Engberg, P. & Lindskog, S. (1984). *FEBS Lett* **170**, 326-330.

28. Eriksson, A. E., Jones, T. A. & Liljas, A. (1988). *Proteins* **4**, 274-282.

29. Ernst, R. R. (1987). *Priniples of Nuclear Magnetic Resonance in One and Two Dimensions*. New York: Oxford Science Publications

30. Fisher, S. Z., Maupin, C. M., Budayova-Spano, M., Govindasamy, L., Tu, C., Agbandje-McKenna, M., Silverman, D. N., Voth, G. A. & McKenna, R. (2007). *Biochemistry* **46**, 2930-2937.

31. Furihata, K., Shimotakahara, S., Tashiro, M. (2007). *Magnetic Resonance in Chemistry* **800**.

32. Genis, C., Sippel, K. H., Case, N., Cao, W., Avvaru, B. S., Tartaglia, L. J., Govindasamy, L., Tu, C., Agbandje-McKenna, M., Silverman, D. N., Rosser, C. J. & McKenna, R. (2009). *Biochemistry*.

33. Gottlieb, H. E., Kotlyar, V., and Nudelman, A.M. (1997). *Journal of Organic Chemistry* **62**, 7512-7515.

34. Guerri, A., Briganti, F., Scozzafava, A., Supuran, C. T. & Mangani, S. (2000). *Biochemistry* **39**, 12391-12397.

35. Hakansson, K., Carlsson, M., Svensson, L.A., Liljas, A. (1992). *J Mol Biol* **4**, 1192-1204.

36. Hakansson, K. & Liljas, A. (1994). *FEBS Lett* **350**, 319-322.

37. Hamid, H., Mohamed, A., Maadhah, A.G. (1992). *Handbook of Polymer Degradation*. New York: M. Dekker.

38. Heck, R. W., Tanhauser, S. M., Manda, R., Tu, C., Laipis, P. J. & Silverman, D. N. (1994). *J Biol Chem* **269**, 24742-24746.

39. Hilvo, M., Baranauskiene, L., Salzano, A. M., Scaloni, A., Matulis, D., Innocenti, A., Scozzafava, A., Monti, S. M., Di Fiore, A., De Simone, G., Lindfors, M., Janis, J., Valjakka, J., Pastorekova, S., Pastorek, J., Kulomaa, M. S., Nordlund, H. R., Supuran, C. T. & Parkkila, S. (2008). *J Biol Chem* **283**, 27799-27809.

40. Hughes, A. D. (2004). *J Renin Angiotensin Aldosterone Syst* **5**, 155-160.

41. Jonsson, B. M., Hakansson, K. & Liljas, A. (1993). *FEBS Lett* **322**, 186-190.

42. Kernohan, J. C. (1966). *Biochim Biophys Acta* **118**, 405-412.

43. Laskowski, R. A., Moss, D. S. & Thornton, J. M. (1993). *J Mol Biol* **231**, 1049-1067.

44. Leibman, J., Gotch, F. A. & Edelman, I. S. (1960). *Circ Res* **8**, 907-912.

45. Lesburg, C. A., Lloyd, M. D., Cane, D. E. & Christianson, D. W. (1995). *Protein Sci* **4**, 2436-2438.

46. Liang, Z., Xue, Y., Behravan, G., Jonsson, B. H. & Lindskog, S. (1993). *Eur J Biochem* **211**, 821-827.

47. Liljas, A., Hakansson, K., Jonsson, B. H. & Xue, Y. (1994). *Eur J Biochem* **219**, 1-10.

48. Lindahl, M., Vidgren, J., Eriksson, E., Habash, J., Harrop, S., Helliwell, J., Liljas, A., Lindeskog, M., and Walker, N. (1991). *Carbonic Anhydrase*. VCH, Weinheim.

49. Lindskog, S. (1997). *Pharmacol Ther* **74**, 1-20.

50. Lindskog, S., and Silverman, D.W. (2000). *The Carbonic Anhydrases -- New Horizons*.

51. Lindskog, S., Engberg, P., Forsman, C., Ibrahim, S. A., Jonsson, B. H., Simonsson, I. & Tibell, L. (1984). *Ann N Y Acad Sci* **429**, 61-75.

52. Lindskog, S., Henderson, L.E., Kannan, K.K., Liljas, A., Nyman, P.O., and Strandberg, B. (1971). *Carbonic Anhydrase Enzymes*. New York: Academic Press.

53. Maren, T. H., Rayburn, C. S. & Liddell, N. E. (1976). *Science* **191**, 469-472.

54. Maren, T. H. & Wiley, C. E. (1968). *J Med Chem* **11**, 228-232.

55. Maren, T. H., Wynns, G. C. & Wistrand, P. J. (1993). *Mol Pharmacol* **44**, 901-905.

56. Masereel, B., Rolin, S., Abbate, F., Scozzafava, A. & Supuran, C. T. (2002). *J Med Chem* **45**, 312-320.

57. McNae, I. W., Kan, D., Kontopidis, G., Patterson, A., Taylor, P., Worrall, L. and Walkinshaw, M.D. (2005). *Crystallogr. Rev.* **11**, 61-71.

58. McPherson, A. (1982). *Preparation and Analysis of Protein Crystals*. New York: John Wiley and Sons.

59. Messerschmidt, A. (2001). *Handbook of metalloproteins*. Chichester ; New York: Wiley.

60. Murakami, H. & Sly, W. S. (1987). *J Biol Chem* **262**, 1382-1388.

61. Nienaber, V. L., Richardson, P. L., Klighofer, V., Bouska, J. J., Giranda, V. L. & Greer, J. (2000). *Nat Biotechnol* **18**, 1105-1108.

62. Noda, I., Ozaki, Y. (2004). *Two-dimensional correlation spectroscopy applications in vibrational and optical spectroscopy*. Hichester, West Sussex: John Wiley and Sons.

63. Otwinowski, Z. a. M., W. (1997). *Processing of X-ray Diffraction Data Collected in Oscillation Mode*. New Haven, CT: Yale University.

64. Ozaki, Y., Czarnik-Matusewicz, B., Sasic, S. (2001). *The Japan Society for Analytical Chemistry* **17**, 663-666.

65. Parkkila, S. & Parkkila, A. K. (1996a). *Duodecim* **112**, 2383-2388.

66. Parkkila, S. & Parkkila, A. K. (1996b). *Scand J Gastroenterol* **31**, 305-317.

67. Pastorek, J., Pastorekova, S., Callebaut, I., Mornon, J. P., Zelnik, V., Opavsky, R., Zat'ovicova, M., Liao, S., Portetelle, D., Stanbridge, E. J. & et al. (1994). *Oncogene* **9**, 2877-2888.

68. Pastorekova, S., Parkkila, S., Pastorek, J. & Supuran, C. T. (2004). *J Enzyme Inhib Med Chem* **19**, 199-229.

69. Pastorekova, S. a. P., J. (2004). *Carbonic Anhydrase. Its Inhibitors and Activators*. CRC Press.

70. Pertini, I., Canti, G., Luchinat, C., and Mani, F. (1981). *Journal of the American Chemical Society* **103**, 7784-7788.

71. Pocker, Y. & Sarkanen, S. (1978). *Adv Enzymol Relat Areas Mol Biol* **47**, 149-274.

72. Pocker, Y. & Stone, J. T. (1968). *Biochemistry* **7**, 2936-2945.

73. Pocker, Y. & Tanaka, N. (1978). *Science* **199**, 907-909.

74. Raghunand, N., He, X., van Sluis, R., Mahoney, B., Baggett, B., Taylor, C. W., Paine-Murrieta, G., Roe, D., Bhujwalla, Z. M. & Gillies, R. J. (1999). *Br J Cancer* **80**, 1005-1011.

75. Rowlett, R. S., Gargiulo, N. J., 3rd, Santoli, F. A., Jackson, J. M. & Corbett, A. H. (1991). *J Biol Chem* **266**, 933-941.

76. Schuttelkopf, A. W. & van Aalten, D. M. (2004). *Acta Crystallogr D Biol Crystallogr* **60**, 1355-1363.

77. Segel, I. (1975). *Enzyme Kinetics: Behavior and Analysis of Rapid Equilibrium and Stead-State Enzyme Systems*. New York: Wiley-Interscience.

78. Sheldrick, G. M. (2008). *Acta Crystallogr A* **64**, 112-122.

79. Silverman, D. N. (1982). *Methods Enzymol* **87**, 732-752.

80. Sly, W. S., Hewett-Emmett, D., Whyte, M. P., Yu, Y. S. & Tashian, R. E. (1983). *Proc Natl Acad Sci U S A* **80**, 2752-2756.

81. Sly, W. S. & Hu, P. Y. (1995). *Annu Rev Biochem* **64**, 375-401.

82. Stams, T. & Christianson, D. W. (2000). *EXS* 159-174.

83. Stams, T., Nair, S. K., Okuyama, T., Waheed, A., Sly, W. S. & Christianson, D. W. (1996). *Proc Natl Acad Sci U S A* **93**, 13589-13594.

84. Stubbs, M., McSheehy, P. M., Griffiths, J. R. & Bashford, C. L. (2000). *Mol Med Today* **6**, 15-19.

85. Supuran, C. T., and Manole, G. (1999). *The Carbonic Anhydrase Inhibitors: Syntheses, REactions and Therapeutical Applications*. Bucharest: Romanian Academy Publishing House.

86. Supuran, C. T., and Scozzafava, A. (2000). *Expert Opinion on Therapeutic Patents* **10**, 575-600.

87. Supuran, C. T., Briganti, F., Tilli, S., Chegwidden, W. R. & Scozzafava, A. (2001). *Bioorg Med Chem* **9**, 703-714.

88. Supuran, C. T., Scozzafava, A. & Conway, J. (2004). *Carbonic anhydrase : its inhibitors and activators*. Boca Raton: CRC Press.

89. Supuran, C. T., Scozzafava, A., and Casini, A. (2003). *Medicinial Research Reviews* **23**, 146-189.

90. Supuran, C. T., Scozzafava,A., and Casini, A (2002). *Expert Opinion on Therapeutic Patents* **12**.

91. Svastova, E. (2004). *FEBS Lett* **577**, 439-445.

92. Svastova, E., Hulikova, A., Rafajova, M., Zat'ovicova, M., Gibadulinova, A., Casini, A., Cecchi, A., Scozzafava, A., Supuran, C. T., Pastorek, J. & Pastorekova, S. (2004). *FEBS Lett* **577**, 439-445.

93. Taylor, P. W., King, R. W. & Burgen, A. S. (1970). *Biochemistry* **9**, 3894-3902.

94. Thiry, A., Dogne, J. M., Masereel, B. & Supuran, C. T. (2006). *Trends Pharmacol Sci* **27**, 566-573.

95. Thompson, J. D., Higgins, D.G., and Gibson, T.J. (1994). *Nucleic Acids Res* **22**, 4673-4680.

96. Thorslund, A. & Lindskog, S. (1967). *Eur J Biochem* **3**, 117-123.

97. Tiller, P. R., Romanyshyn, L. A. & Neue, U. D. (2003). *Anal Bioanal Chem* **377**, 788-802.

98. Verdonk, M. L., Chessari, G., Cole, J. C., Hartshorn, M. J., Murray, C. W., Nissink, J. W., Taylor, R. D. & Taylor, R. (2005). *J Med Chem* **48**, 6504-6515.

99. Vidgren, J., Liljas, A. & Walker, N. P. (1990). *Int J Biol Macromol* **12**, 342-344.

100. Vilenchik, L. Z., Griffith, J.P., St Clair, N., Navia, M.A. and Margolin, A.L. (1998). *J. Am. Chem. Soc.* **120**, 4290-4294.

101. Vukovic, V. & Tannock, I. F. (1997). *Br J Cancer* **75**, 1167-1172.

102. Vullo, D., Innocenti, A., Nishimori, I., Pastorek, J., Scozzafava, A., Pastorekova, S. & Supuran, C. T. (2005). *Bioorg Med Chem Lett* **15**, 963-969.

103. Wingo, T., Tu, C., Laipis, P. J. & Silverman, D. N. (2001). *Biochem Biophys Res Commun* **288**, 666-669.

104. Wu, N. a. P., E.F. (2002). *Journal of Biological Chemistry* **277**, 28080-28087.

105. Wu, W. (2003). 2003 NMR User Training Course, edited by N. P. f. G. M. H.-F. N. C. Facility.

106. Yoshioka, S., Stella, V.J. (2002). *Stability of drugs and dosage forms*. New York: Kluwer Academic.

BIOGRAPHICAL SKETCH

Jeanne Quirit was born in Los Angeles, California. She matriculated in the University of Florida in the fall of 2004 as an undergraduate. She received her Bachelor of Science in Biochemistry and Molecular Biology as a part of the Interdisciplinary Studies Program and a minor in Art History in May of 2008. She joined the McKenna lab in January of 2007 and initially did her work on *Aaedes aegypti* carbonic anhydrase and became a University Scholar later that year. Her love for research and the lab prompted her to continue her research as a graduate student following her graduation from college. She enjoys music, art, and astronomy. Following her graduate studies, Jeanne hopes to attend medical school.